

MODERATE ACCUMULATION OF TDP-43 IN NEURONS IS
SUFFICIENT TO CAUSE ADULT-ONSET MOTOR NEURON DISEASE

by

William W. Tsao

A dissertation submitted to Johns Hopkins University in conformity with the
requirements for the degree of Doctor of Philosophy

Baltimore, Maryland

March, 2015

© 2015 William W. Tsao

All Rights Reserved

ABSTRACT

Cytoplasmic aggregation of TAR DNA-binding protein 43 (TDP-43), accompanied by its nuclear clearance, is a key common pathological hallmark of Amyotrophic Lateral Sclerosis (ALS) and Frontotemporal Lobar Degeneration (FTLD). Mutations in *TARDBP* (the gene encoding TDP-43) linked to familial and sporadic ALS established this essential RNA binding protein to play a central role in the pathogenesis of ALS and FTLD. While most mutations cluster within the C-terminal, prion-like domain of TDP-43, a few are found within the 3' untranslated region (3' UTR) where TDP-43 binds and regulates the level of its own mRNA. ALS cases harboring the 3' UTR mutation exhibited modest elevation of TDP-43, possibly because the mutation compromised the ability of TDP-43 to downregulate its own transcript.

To determine whether modest increase of TDP-43 is sufficient to cause motor neuron disease, two lines of transgenic mice that accumulate modest levels of TDP-43 in the nervous system are generated and characterized. One of these lines, S97, expressed *TARDBP* carrying the ALS associated missense mutation (corresponding to the mutant G298S protein), whereas the other line, W2, expressed wild-type human *TARDBP*. S97 and W2 transgenic mice survive to adulthood, gain weight appropriately before plateauing, exhibit a progressive loss of strength, and lose large motor axons in their adult life. Also, S97 and W2 transgenic mice display adult-onset muscle degeneration and neuromuscular junction and motor end-plate abnormalities. Significantly, a percentage of S97 and W2 transgenic mice progress to paralysis late in life. The S97 and W2 lines represent the first transgenic TDP-43 lines with mice that exhibit motor neuron degeneration leading to paralysis in late adulthood. As such, these mouse lines will be

useful to further clarify disease mechanisms and for testing therapeutic strategies to attenuate neurodegeneration in ALS.

Advisor: Dr. Philip C. Wong

Readers: Dr. Philip C. Wong and Dr. Joseph L. Mankowski

ACKNOWLEDGMENTS

I would first like to thank my thesis advisor, Phil Wong, without whom none of this work would have been possible. His support and encouragement carried me through all of the trials of graduate training, and I will always be grateful.

Additionally, I would like to thank the members of my thesis committee, Drs. Joseph Mankowski, Juan Troncoso, and Lee Martin. Their suggestions and encouragement were invaluable to this work.

Special thanks to administrative staff in the Cellular and Molecular Medicine program and in the Johns Hopkins Division of Neuropathology, who kept all things running smoothly.

Finally, thank you to those who were at my side throughout this journey: my wife Becky, my parents and sister, and my colleagues – and friends – in Dr. Wong's laboratory.

TABLE OF CONTENTS

Chapter 1: Introduction	1
1. The Motor Neuron Diseases and Amyotrophic Lateral Sclerosis	2
2. The Genetics of ALS	4
3. The Identification of TDP-43 in ALS Patient Samples	5
4. TDP-43 Pathology Links ALS and Frontotemporal Lobar Degeneration	6
5. ALS- and FTL-Linked Mutations in TARDBP	7
6. Initial Sets of Transgenic Rodent Models of TDP-43	9
Chapter 2: Generation and Characterization of Mouse Models Expressing Moderate Levels of Human TDP-43	14
1. Introduction	15
2. Materials and Methods	17
3. Results	24
4. Discussion	29
Chapter 3: Identification of Pathways Impacted by Modest Increase of TDP-43 in Neurons: Transcriptome Analysis of Spinal Cords from S97 and W2 Mice	32
1. Introduction	33
2. Materials and Methods	34
3. Results	35
4. Discussion	37
Chapter 4: Concluding Remarks	40
Figures	44
Supplemental Figures	76
References	80
Curriculum Vitae	101

CHAPTER 1: INTRODUCTION

The Motor Neuron Diseases and Amyotrophic Lateral Sclerosis

The motor neuron diseases (MND), including Amyotrophic Lateral Sclerosis (ALS), are chronic, progressive illnesses characterized clinically by severely disabling features involving motor systems – weakness, muscle atrophy, and, in ALS, spasticity – and pathologically by the presence of intracellular protein aggregates (inclusions), alterations in axonal transport, and death of motor neurons. There is a relatively selective involvement of lower motor neurons in MND, and in classical ALS, both upper and lower motor neurons are affected. The majority of MND cases appear to be sporadic, but a small percentage of patients have a familial history. Some forms of the disease are autosomal dominant, while others are recessive. Studies have shown that in some instances, the presence of specific gene products confers risk for disease. Although symptomatic treatments are available, there are no current effective mechanism-based therapies (Wong et al., 2002; Bruijn et al., 2004). Recent research, particularly studies utilizing animal models, has provided insights into mechanisms of these disorders and identified new potential targets for therapy, thereby facilitating the design and testing of novel treatment strategies.

ALS was originally described by Charcot in 1874, and in the United States is commonly known as Lou Gehrig's Disease, after the Major League Baseball player whose career was shortened by the disease (Rowland and Shneider, 2001). It is the most common adult onset form of MND, with a prevalence of approximately 2-3 per 100,000 people (Cleveland and Rothstein, 2001; Julien, 2001). Each year in the United States, in excess of 5000 people are diagnosed with ALS. The principal clinical signs of ALS include: progressive limb weakness, which may be symmetrical or asymmetrical; atrophy

of appendicular, bulbar, and respiratory muscles; and spasticity. The paralysis/muscle atrophy and spasticity are the result of degeneration of motor neurons in the spinal cord/brain stem and motor cortex, respectively. There is variation in the clinical presentation as some patients display weakness starting in the extremities while others first present with speech or swallowing abnormalities. Furthermore, some exhibit frontotemporal dementia or Parkinsonism yet others do not. The onset of this illness is typically in the 5th or 6th decade of life, and affected individuals usually die within 2-5 years of appearance of symptoms. It is estimated that 5-10% of ALS cases have a family history of the disease (fALS), while the other cases are characterized as sporadic ALS (sALS). While the causes of the majority of cases of ALS have yet to be identified, shared features of the clinical presentations and pathologies occurring in both sporadic and familial cases suggest the existence of common disease mechanisms.

The identification of causative mutations in specific genes in cases of human MND, including familial ALS (fALS) and spinal muscular atrophy (SMA) (Rosen et al., 1993; Sreedharan et al., 2008; Kabashi et al., 2008; Vance et al., 2009; Kwiatkowski et al., 2009; Puls et al., 2003; Lefebvre et al., 1995), has provided new opportunities to investigate the molecular participants in disease processes using transgenic and gene targeting approaches (Wong et al., 2002; Bruijn et al., 2004). In autosomal dominant fALS, the mutant proteins often acquire toxic properties that directly or indirectly impact on the functions and viability of neurons (Julien, 2001), and introduction of mutant genes into mice reproduces some features of these diseases (Wong et al., 1995; Bruijn et al., 1997; Dal Canto and Gurney, 1994; Laird et al., 2008). In contrast, autosomal recessive diseases like SMA, which usually lack the functional protein encoded by the mutant gene

(Survival Motor Neuron (SMN) in SMA), can often be modeled by gene targeting strategies (Wong et al., 2002).

In models of MND, therapeutic manipulations, manipulation of expression of selected genes in specific cell populations (Subramaniam et al., 2002; Lambrechts et al., 2003), creation of chimeric animals to test whether abnormalities are cell autonomous (Clement et al., 2003), administration of trophic factors to prevent trophic cell death (Koliatsos et al., 1993; Henderson et al., 1994), and testing of a variety of drug therapies (Rothstein, 2003; Kriz et al., 2003; Zhu et al., 2002; Rothstein et al., 2005) have been evaluated to ameliorate phenotypes and thus provide insights into disease mechanisms and potential treatment strategies.

The Genetics of ALS

Approximately 5-10% of cases of ALS are familial, and, in the majority of these cases, the disease is inherited as an autosomal dominant (Wong et al., 2002; Bruijn et al., 2004; Cleveland and Rothstein, 2001). In 1993, it was discovered that mutations in the *Cu/Zn superoxide dismutase (SOD1)* gene, were associated with about 20% of fALS and 1% of sALS (Rosen et al., 1993; Jones et al., 1993). Since then, several other genes or risk factors have been identified. *Dynactin p150^{glued}* has been linked to autosomal dominant fALS (Puls et al., 2003) and may, as an allelic variant, serve as a risk factor (Munch et al., 2004). Autosomal recessive deletion mutations have been identified in *ALS2* which encodes Alsin, a protein that regulates GTPases (Hadano et al., 2001; Yang et al., 2001). In a rare autosomal dominant form of juvenile ALS, mutations have been identified in the gene (*SETX*) that encodes senataxin (Chen et al., 2004), which contains a

DNA/RNA helicase domain with homology to other proteins known to have roles in the processing of RNA (Moreira et al., 2004). Following an observation that deletion of the hypoxia response element in the promoter of the *vascular endothelial growth factor (VEGF)* gene causes degeneration of motor neurons in mice (Oosthuysen et al., 2001), it has been reported that individuals homozygous for certain haplotypes in the VEGF promoter have an increased risk for ALS (Lambrechts et al., 2003; Cleveland, 2003). Discoveries of additional genes linked to ALS, including *OPTN* (Maruyama et al., 2010), *VCP* (Johnson et al., 2010), *UBQLN2* (Deng et al., 2011), *FUS* (Vance et al., 2009; Kwiatkowski et al., 2009), *Matrin 3* (Johnson et al., 2014), *Profilin 1* (Wu et al., 2012), *TUBA4A* (Smith et al., Neuron 2014) and *C9ORF72* (DeJesus-Hernandez et al., 2011; Renton et al., 2011) as well as risk factors such as Ataxin-2 polyglutamine expansion (Eliden et al., 2010), provide further opportunities to unravel this complex motor neuron disease in the future.

The Identification of TDP-43 in ALS Patient Samples

In 2006, the field of ALS research was pushed in a new direction when the protein in the inclusions commonly seen in most ALS patient samples was discovered to be TAR DNA-binding protein 43 (TDP-43) (Neumann et al., 2006, Arai et al., 2006). In ALS patients without SOD1 mutations, TDP-43 was shown to colocalize with ubiquitin in tau-negative, a-synuclein-negative neuronal and glial cytoplasmic inclusions (Mackenzie et al., 2007). In addition, the presence of phosphorylated 25-kDa TDP-43 fragments and the partial clearance of nuclear TDP-43 were observed (Neumann et al., 2006). Initial thoughts, then, were that TDP-43 proteinopathy – the presence of cytoplasmic

aggregation of TDP-43 and the loss of functional TDP-43 from the nucleus – could cause neuronal dysfunction.

TDP-43, encoded by the chromosome 1 gene *TARDBP*, is a 43-kDa predominately nuclear protein, thought to bind to DNA and RNA and have roles in transcription regulation and RNA processing (Lagier-Tourenne and Cleveland, 2009). TDP-43 belongs to the hnRNP family, and contains two RNA-recognition motifs, an NLS and NES to facilitate nucleocytoplasmic shuttling, and a highly conserved, glycine-rich C-terminal domain thought to mediate protein-protein interactions (Ayala et al., 2008; D’Ambrogio et al., 2009; Barnada et al., 2010). It has been shown to be widely expressed in many tissues in humans and rodents (Buratti and Baralle, 2008). It was first identified in 1995 as a protein that could bind to and repress transcription of HIV transactive response DNA (Ou et al., 1995). Later it became known as a protein that could regulate splicing. It was discovered that TDP-43 facilitated skipping of exon 9 of the *cystic fibrosis transmembrane conductance regulator* gene by binding to UG-rich RNA (Buratti et al., 2004; Ayala et al., 2005). Also, it was discovered that TDP-43 could enhance the inclusion of exon 7 in *SMN2* pre-RNA (Bose et al., 2008).

TDP-43 Pathology Links ALS and Frontotemporal Lobar Degeneration

TDP-43 pathology was also identified in cortical samples from a subset of patients with Frontotemporal lobar degeneration (FTLD) (Neumann et al., 2006, Arai et al., 2006). This subset of patients is now recognized as having “FTLD with TDP-43” (FTLD-TDP), and together with patients with FTLD with tau (FTLD-tau) and with FTLD with FUS (FTLD-FUS), represents almost all patients with FTLD (Mackenzie et al.,

2010). The shared pathological hallmark of TDP-43 inclusions, along with observations that ALS and FTLN can coexist in patients (Lomen-Hoerth et al., 2002, Gendron et al., 2013), led to the idea that ALS and FTLN-TDP were on the same disease spectrum (Neumann et al., 2006).

The term FTLN covers a clinically and pathologically diverse group of disorders resulting from frontal or anterior temporal lobe degeneration of the brain (Bennion Callister and Pickering-Brown, 2014). FTLN is second only to Alzheimer's disease as the most common cause of dementia in those younger than 65 years old, with a prevalence of approximately 10-30 per 100,000 people aged 45-65 years old (Sieben et al., 2012). Clinically, patients with FTLN typically present with one of three syndromes: behavioral-variant frontotemporal dementia (bvFTD), presenting with personality, behavior changes, and often apathy with disinhibition; semantic dementia (SD), presenting with a fluent, anomia aphasia; or progressive nonfluent aphasia (PNFA), presenting often with apraxia (Rabinovici and Miller, 2010). bvFTD is the variant most commonly associated with ALS.

ALS- and FTLN-Linked Mutations in *TARDBP*

The discovery that TDP-43 inclusions were a pathologic hallmark of ALS and FTLN-TDP encouraged several groups to screen large cohorts of ALS and FTLN patients for mutations in *TARDBP* (Gendron et al., 2013). Beginning in 2008, several *TARDBP* mutations were discovered, in both fALS and sALS patients (Kabashi et al., 2008; Kuhnlein et al., 2008; Rutherford et al., 2008; Sreedharan et al., 2008; Van Deerlin et al.,

2008; Yokoseki et al., 2008). Mutations in *TARDBP* were also discovered in patients with FTLN (Benajiba et al., 2009; Borroni et al., 2010; Gitcho et al., 2009).

Most of these *TARDBP* mutations were found in the coding regions, correlating with single amino acid substitutions in the glycine-rich C-terminal domain (Gendron et al., 2013). The effect of these missense mutations has been studied in several model systems. TDP-43 with the Q331K mutation was shown to cause increased accumulation of TDP-43 fragments in CHO cells and developmental delay in chick embryos (Sreedharan et al., 2008). Increased accumulation of TDP-43 fragments was also found in lymphoblastoid cells from patients with the G348C, R361S, N390D, and N390S variants (Kabashi et al., 2008). In various cell culture models, TDP-43 missense mutations caused increased TDP-43 cytoplasmic aggregation (Barmada et al., 2010; Budini et al., 2012), possibly in conjunction with stress granule formation (Liu-Yesucevitz et al., 2010; Parker et al., 2012). In yeast, the TDP-43 mutations Q331K, M337V, Q343R, N345K, R361S, and N390D increase TDP-43 aggregation and yeast cell death (Johnson et al., 2009). Though the effect of TDP-43 missense mutations in driving increased aggregation is well established in these model systems, the mechanism by which TDP-43 missense mutations can cause neuronal toxicity remains unclear.

In addition to the coding region mutations found in *TARDBP*, an additional interesting mutation (2076 G to A) was found in a noncoding area – the 3' untranslated region (3'UTR) – in three patients with ALS and/or FTLN-TDP (Gitcho et al., 2009). This mutation caused these patients to have increased levels of *TARDBP* mRNA compared to normal controls and to patients with a *TARDBP* coding region mutation. Initially the reasons for this increased expression level were unclear. However, it was

later discovered that TDP-43 tightly regulates the level of its own transcript, by binding to a region in the 3'UTR and initiating transcript destruction by alternative splicing and nonsense-mediated decay (Polymenidou et al., 2011) or other mechanisms (Ayala et al., 2011). Since the 2076 G to A mutation lies within the *TARDBP* region where TDP-43 likely binds (Ayala et al., 2011), it is possible that a disruption of binding leads to the disruption of autoregulation, that causes increased *TARDBP* transcript levels in these ALS/FTLD-TDP patients.

Initial Sets of Transgenic Rodent Models of TDP-43

To understand the pathogenic mechanisms of mutant TDP-43 underlying ALS, it was important to clarify first the physiological roles of TDP-43 in the nervous system. To address this issue, investigators used a gain-of-function approach to generate transgenic mice overexpressing either wild type or ALS-linked mutant TDP-43 using a neuronal-specific promoter (eg., Thy1.2), an inducible promoter (eg., tTA-tetOff) or ubiquitous promoter (eg. mouse PrP or endogenous human TDP-43). These mouse lines may also serve as good models for ALS/FTLD-TDP with noncoding-region mutations, as another way to disrupt TDP-43 autoregulation is to express exogenous TDP-43 protein (Lee et al., 2012).

Several groups (Wegorzewska et al., 2009; Stallings et al., 2010; Xu et al., 2010; Xu et al., 2011; Arnold et al., 2013) generated lines of mice expressing human TDP-43 (hTDP-43) under the control of the murine prion protein promoter (moPrP). This promoter drives protein expression in the brain, spinal cord, and heart, and to a lesser extent, in skeletal muscle, lung, liver, and kidney (Borchelt et al., 1996). Each of the

moPrP mouse lines expressed either wild-type or the ALS-linked mutants A315T or M337V encoded by the human *TARDBP* cDNA. In almost every moPrP-driven line, an elevated level of hTDP-43 in the spinal cord or brain led to motor deficits and relatively early lethality. High-expressing mouse lines displayed a more severe and lethal phenotype, and founders with very high level of protein accumulation died before reaching sexual maturity. While intranuclear aggregates of TDP-43 and diffuse cytoplasmic ubiquitin staining were common to many lines, cytoplasmic aggregates of TDP-43 colocalized with ubiquitin were rare and generally only detectable using an antibody to phosphorylated TDP-43. Although mice expressing low level of the transgene (hTDP-43^{WT}, line 21) showed no motor deficits (Stallings et al., 2010), mice expressing high level of wild-type hTDP-43 (hTDP-43^{WT} homozygous line, Xu et al., 2010) showed a very similar motor phenotype to the comparably-expressing homozygous mutant M337V line (Xu et al., 2011). Indeed, there appeared to be little difference between lines expressing wild-type hTDP-43 and mutant hTDP-43 driven by the moPrP promoter to comparable levels. In addition, investigators studying these moPrP lines needed to be careful for off-target effects, as in the A315T line (Wegorzewska et al., 2009), moPrP-driven overexpression of TDP-43 in myenteric plexes resulted in gut ischemia and death (Guo et al., 2012; Esmaili et al., 2013; Hatzipetros et al., 2014).

In addition to our group (Shan et al., 2010), Wils and co-workers (Wils et al., 2010; Janssens et al., 2013) generated TDP-43 mouse lines under the control of a modified murine Thy1 promoter. The Thy1.2 cassette drives expression almost exclusively in neurons (Vidal et al., 1990; Caroni, 1997). The highest-expressing mouse lines, like Shan's W1 and Wils's TAR4/4 (both expressing hTDP-43^{WT}), and Janssens's

Mt-TAR6/6 (expressing hTDP-43^{M337V}) progressed within 1 month to paralysis and death. The lower expressing lines had milder phenotypes, but did not result in paralysis save Janssens's line Mt-TAR6. In Mt-TAR6, however, mouse-to-mouse variability was high: 5% of mice got paralyzed, but the onset of paralysis ranged from 3 to 14 months (Janssens et al., 2013). The predominant histologic finding in these mouse lines was the presence of cytoplasmic inclusions containing mitochondria but not TDP-43. In addition, investigators studying these Thy1 mouse lines needed to be careful about making comparisons between lines. As has been noted previously, mice generated using the Thy1.2 cassette exhibit line-to-line variability in the expression pattern of different populations of neurons (Wegorzewska and Baloh, 2010; Feng et al., 2000).

Two groups used the Ca²⁺/Calmodulin-dependent kinase II (CaMKII) promoter, either in constitutive (Tsai et al., 2010) or inducible (Igaz et al., 2009) fashion, to drive expression of TDP-43 in the hippocampus and cortex. That overexpression of the mouse TDP-43 in the forebrain led to behavioral and motor deficits and cortical neuron loss (Tsai et al., 2010) indicated that mouse TDP-43 (mTDP-43) was toxic when overexpressed in mice. This finding supported the view that elevated hTDP-43 is toxic in mice because of an elevated expression level and not because hTDP-43 acts like a nonfunctional or dysfunctional protein in a mouse background. In contrast, Igaz and co-workers (Igaz et al., 2010) documented that overexpression of hTDP-43^{WT} in cortical neurons downregulated the level of mouse TDP-43, presumably due to TDP-43 autoregulation (Ayala et al., 2011; Polymenidou et al., 2011) in those neurons, suggesting that expression of hTDP-43 is toxic because it suppresses the level of mouse TDP-43.

Recognizing the toxicity of highly elevated TDP-43 levels and the importance of expression pattern of the transgene, Swarup and co-workers (Swarup et al., 2011) used the TDP-43-containing gene fragment from a human bacterial artificial chromosome to drive transgene expression in a low-level pattern mimicking the endogenous expression pattern. The resulting hTDP-43^{WT}, hTDP-43^{A315T}, and hTDP-43^{G348C} lines all had hTDP-43 transcript levels close to 3 times that of the mouse TDP-43 transcript levels in the spinal cord, though it appears that the total TDP-43 level in spinal cord protein extracts are much higher in the mutant lines as compared to that of the wild-type line. All lines exhibit behavioral and motor deficits at 7-12 months of age. Spinal cord sections of 10 month old hTDP-43^{G348C} mice show some punctate staining of hTDP-43 colocalized with ubiquitin, a finding which is not observed in hTDP-43^{WT} mice. Additionally, 25- and 35-kDa fragments are detected in the spinal cord lysate of 10 month old hTDP-43^{G348C} mice, but not of younger hTDP-43^{G348C} mice or of hTDP-43^{WT} mice. There does appear to be significant additional pathological findings associated with the G348C mutation, but it is unknown whether these same findings would occur in hTDP-43^{WT} mice with a more comparable protein level.

Using a similar BAC transgenic approach, a rat model of TDP-43 overexpression was generated (Zhou et al., 2010). This model was unique in that the 2 rat founders expressing hTDP-43^{WT} did not show a paralytic phenotype up to 200 days, but the 3 rat founders expressing hTDP-43^{M337V} at comparable levels developed paralysis by 29 days. The investigators also used a tetracycline-inducible system coupled with a CAG promoter to drive ubiquitous expression of hTDP-43^{M337V} postnatally, and found that rats in the lower-expressing Line 7 were initially asymptomatic but progressed to paralysis and

death by 55 days. While neuronal loss was observed only in the hTDP-43^{M337V} lines, diffuse nuclear and cytoplasmic phosphorylated TDP-43 staining was detected in both mutant and hTDP-43^{WT} rats.

Taken together, these initial sets of TDP-43 transgenic studies revealed several important observations. First, overexpression of human wild type or ALS-linked mutant TDP-43, or mouse TDP-43, was toxic in a dose-dependent manner in mice. However, the mechanism by which toxicity occurred, whether because the wild-type or mutant hTDP-43 was itself toxic in mice or because nonfunctional hTDP-43 was replacing functional mouse TDP-43, was unclear. In the only TDP-43 rat model study, overexpression of the ALS-linked mutant TDP-43, but not the human wild type TDP-43, was toxic. Secondly, the phenotype of each mouse line was sensitive to the pattern of exogenous TDP-43 expression. Thirdly, cytoplasmic aggregation of TDP-43 did not appear to be critical to develop a disease phenotype.

**CHAPTER 2: GENERATION AND CHARACTERIZATION OF MOUSE
MODELS EXPRESSING MODERATE LEVELS OF HUMAN TDP-43**

INTRODUCTION

Cytoplasmic aggregation of TDP-43 accompanied by its nuclear clearance – termed TDP-43 proteinopathy – is a key common pathological hallmark of ALS-FTLD (Neumann et al., 2006). However, the pathogenic mechanism(s) underlying TDP-43 proteinopathy in this disease spectrum remains elusive. To address this important question, we employed a transgenic mouse approach to generate and characterize lines of mice expressing ALS-linked mutant TDP-43.

By the Fall of 2008, several groups had begun developing TDP-43 transgenic mouse models, but none had yet been published. In our own group, Xiu Shan had generated and was characterizing several lines of TDP-43 transgenic mice, denoted W1, W2, and W3. These lines were all generated using a construct with the wild-type human *TARDBP* cDNA under the control of a murine Thy1.2 promoter (Vidal et al., 1990). This promoter had been shown to allow transgene expression in mice in a robust, neuron-specific manner, starting 6-12 days after birth (Caroni, 1997).

Shan's lines expressing wild-type human TDP-43 were initially expected to be control lines, for future experiments on lines expressing human TDP-43 with ALS-linked mutations. This strategy followed the example of the SOD1 mouse models, in which expression of ALS-linked mutant human SOD1 caused motor neuron disease but mice expressing of wild-type human SOD1 at similar or higher levels were phenotypically normal (Wong et al., 1995). Unexpectedly, whether because the wild-type human TDP-43 was itself toxic in mice or because nonfunctional human TDP-43 was replacing functional mouse TDP-43, transgenic mice in lines W1, W2, and W3 developed motor neuron disease (Shan et al., 2010). Transgenic mice in the highest-expressing line, W1,

had phenotypes so severe that every transgenic mouse perished before the age of 3 weeks. Shan chose to characterize the intermediate-expressing line, W3. Transgenic W3 mice had less severe motor neuron disease phenotypes than W1 mice, but had interesting pathologic findings including mitochondrial cytoplasmic aggregates in some motor neurons and intranuclear aggregates of hTDP-43 that colocalized with FUS/TLS and SC35. Meanwhile, the lowest-expressing line W2, remained uncharacterized.

Given the availability of W2 and W3 transgenic mice in our laboratory, we believed that if we could create a transgenic mouse line in which mice expressed an ALS-linked mutant TDP-43 with an expression level and pattern closely matching mice of either the W2 or W3 lines, we could tease out what additional effects the mutation may have. Ideally the expression level of our newly generated line would match the lowest-expressing wild-type human TDP-43 line, W2. This would presumably mitigate the early phenotype seen in the higher-expressing transgenic TDP-43 mouse lines, which did not model well the adult-onset nature of ALS. For example, transgenic males in the W3 line had a significant early reduction in body weight, which is not thought to be typical of ALS patients who appear to be phenotypically normal until the mid-life onset of disease.

Selection of ALS-Linked Mutant TDP-43

By 2008, several mutations in *TARDBP* had been linked to ALS (Kabashi et al., 2008; Kuhnlein et al., 2008; Rutherford et al., 2008; Sreedharan et al., 2008; Van Deerlin et al., 2008; Yokoseki et al., 2008). The familial G298S variant was chosen for study due to its presence in multiple affected members of an ALS family, who had typical clinical courses characterized by mid-life onset – at ages 41, 47, 48, 52, and 60 – and rapid

disease progression – with death at years 1, 1, 2, 2, and 4 from symptom onset (Van Deerlin et al., 2008). Additionally, histological profiles performed on these patients were significant for TDP-43-positive neuronal inclusions in upper and lower motor neurons and other cells in the brain and spinal cord. Also intriguing about the G298S variant was the possibility that the glycine to serine substitution could add a phosphorylation site. This could affect the generation of phospho-TDP-43 fragments, as observed in ALS patient samples (Neumann et al., 2006).

MATERIALS AND METHODS

Generation of Transgenic Mouse Line S97

Site-directed mutagenesis of the wild-type Human *TARDBP* cDNA was performed by PCR overlap extension (Ho et al., 1989), cloning *Sall* sites into both ends of the cDNA while simultaneously generating a G to A substitution in the 1026 position of *TARDBP* (corresponding to a glycine to serine substitution at position 298 in the human TDP-43 protein). The resulting DNA fragment was digested with *Sall* and ligated into the *XhoI* site of pTSC-21, a plasmid containing the Thy1.2 expression cassette (Figure 1) on a pUC18 backbone (courtesy X. Shan). The new plasmid, pTSC-TDP-G298S, was sequenced to confirm the single nucleotide substitution. Expression of Human TDP-43 was confirmed by transfection of the plasmid using Lipofectamine 2000 (Invitrogen) into Neuro-2a cells and immunoblotting (Supplemental Figure 1).

The plasmid pTSC-TDP-G298S was then submitted to the Transgenic Core Laboratory at the Johns Hopkins University School of Medicine for pronuclear injection using the hybrid mouse strain C57B6;SJL. Ninety-seven potential founders were

screened by tail cutting, genomic DNA extraction, and PCR genotyping. Mice tagged S51, S92, and S97 were established as founders and mated with C57B6;SJL/F1 breeder females. Several of the resulting transgenic F1 pups were sacrificed for immunoblotting and immunohistochemical analysis. In addition, genomic DNA was isolated from pups and human *TARDBP* was sequenced, showing the single G to A substitution (Supplemental Figure 2). The line established from founder S97 was determined to be the most promising due to the phenotype and the TDP-43 expression level of transgenic mice in this line. The S97 line was maintained in the hybrid background and phenotypic characterization was started at the F3 generation. All experiments were conducted under an animal use protocol approved by the Animal Care and Use Committee of the Johns Hopkins Medical Institutions.

Genotyping

Mouse tissue for genotyping was obtained via tail cutting or ear punch. Genomic DNA was prepared from tissue via the HotShot technique (Truett et al., 2000). Briefly, tissue was lysed by heating to 95°C for 30 minutes in nuclease-free H₂O with 25mM NaOH and 0.2mM EDTA. An equal volume of nuclease-free H₂O with 40mM Tris-HCl was added, and the resulting solution was used for PCR. The genotyping primer set 5'-CGG AAG ACG ATG GGA CGG TG, 5'-GCC AAA CCC CTT TGA ATG ACC A, and 5'- AAG ATG GCA CGG AAG TCT AAC CAT G, was used to generate a 386 base pair band (spanning *TARDBP* exons 2, 3, and 4) in transgenic mice only and a 241 base pair internal control band in all mice.

Phenotypic Characterization

A cohort of mice in the F3 to F5 generations from the S97 and W2 lines were weighed weekly. The F3 generation in particular was followed to end-stage (death or inability to right from a lateral decubitus position), and survival data was recorded. In addition, development of paralysis was noted in several mice, and images and video was obtained.

A subset of this population was selected for monthly hanging wire tests. Briefly, a mouse was placed on a wire grid, and the grid was shaken to encourage the mouse to grip the wires. The grid was then turned upside down and held level while the time for the mouse to fall was recorded. The end-point was 60 sec, which many of the healthy mice were able to achieve. Each mouse was tested 3 times, with the maximum hang time recorded as the result.

Another subset of mice was studied using the TreadScan System, a high speed camera, and a transparent belt treadmill (CleverSys Inc). Given that training-naïve mice tend to perform the walking task more readily (Beare et al., 2009), mice were tested without training on the treadmill run at 15cm/s. A minimum of 4 complete strides were recorded for each mouse and analyzed for the stride length in each leg.

Immunoblotting

Tissues including cortex, brain stem, cerebellum, spinal cord, sciatic nerve, heart, kidney, and quadriceps muscle were obtained from freshly euthanized mice. Fibrous tissues like muscle and heart were frozen on dry ice, sealed in plastic, and crushed. Non-fibrous tissue and crushed fibrous tissue were homogenized in cold RIPA Buffer with 1%

SDS, protease inhibitor (Roche Complete ULTRA mini tablet + EDTA), and phosphatase inhibitor (Roche PhosStop). Samples were centrifuged at 14,000g at 4°C, and supernatants were saved. Protein concentrations in the supernatants were determined using a BCA assay (Pierce), and 20µg of total protein was loaded into each well of a 10-20% Tris-Glycine gel or a 4-12% Bis-Tris gel (Invitrogen). Protein was transferred to PVDF membrane (Millipore) at 30V for 90 minutes, and then the membrane was blocked for 1 hour with IB blocking buffer: 5% BSA in TBS with 0.1% Tween-20. IB blocking buffer was also used to dilute the primary antibodies (Supplemental Figure 3). Membranes were incubated overnight at 4°C in primary antibody solution, then washed three times with TBS with 0.1% Tween-20, and incubated for 2 hours with secondary antibody (Goat anti-mouse IgG-HRP or Goat anti-rabbit IgG-HRP, Sigma) diluted in blocking buffer. Three more washes with TBS with 0.1% Tween-20 followed, and then membranes were soaked in ECL solution (EMD Millipore Immobilon), dried, and exposed to film (Denville HyBlot). Densitometric analysis was performed using Quantity One software (Biorad).

Tissue Preparation for Sectioning

Mice were anesthetized with an intraperitoneal injection of 15% chloral hydrate. Anesthetization was monitored with limb and corneal reflex checks. Portions of quadriceps muscles were snap-frozen for sectioning. The mice were transcardially perfused with 50-100 mL of cold PBS, and then with fixation buffer (4% Paraformaldehyde in 0.1M Phosphate Buffer, pH 7.4). The L3 and L4 dorsal root ganglia and attached dorsal and ventral roots were identified, removed, placed in fixation buffer

with 2% glutaraldehyde overnight, and then washed in PBS and embedded in Epon. The brain and spinal cord were dissected and separated into right/left halves. One half of each was placed in fixation buffer overnight at 4°C with gentle agitation, and then held in PBS prior to embedding in Paraffin and sectioning. The other half brain, half spinal cord were placed in fixation buffer for 2 hours, and then were switched to sterile PBS with 30% sucrose overnight at 4°C with gentle agitation (12 hours). The sucrose was blotted off and the samples were embedded in O.C.T. Compound (EMS Tissue-Tek) and frozen in isopentane for cryostat sectioning. Gastrocnemius muscles were placed in 30% sucrose overnight at 4°C with gentle agitation, in preparation for sectioning. The remaining mouse tissues were stored in PBS and archived.

Immunohistochemistry for Neural Tissue

Paraffin-embedded brain samples were sectioned in the sagittal axis and spinal cord samples were sectioned in the cross-sectional axis onto slides. Slides used for immunohistochemistry were incubated at 60°C for 30 minutes, then deparaffinized in xylene and ethanol. Antigen retrieval was accomplished by incubating slides for 5 minutes in boiling 10mM sodium citrate buffer (pH 6.0). Slides were cooled to room temperature, and then sections were outlined with an hydrophobic barrier pen (ImmEdge, Vector Labs), and blocked and stained using appropriate primary antibodies (Supplemental Figure 3) and reagents from the Vectastain Elite ABC kit (Vector Labs). Diaminobenzidine exposure was titrated to optimal contrast, sections were counterstained with Mayer's hemalaun, and then dehydration was accomplished using ethanol and xylene.

Dorsal and Ventral Root Analysis

Thick (1 μm) sections of L3 dorsal and ventral roots were cut from Epon blocks, stained with Toluidine blue, and visualized under light microscopy (Olympus). Ventral root images were recorded and processed using ImageJ (NIH), and each axon in the field was manually selected with the tracing tool to obtain the Feret diameter. The Feret diameters of every axon in each ventral root were separated into histogram bins of 0.5 μm each. A bimodal distribution was observed, with “large-diameter axons” taken as those with Feret diameter greater than or equal to 4.5 μm .

Immunofluorescence Analysis of Neuromuscular Junctions

Frozen gastrocnemius muscle was cut into 40 μm longitudinal sections using a freezing sliding microtome (Leica). Sections were separated into wells on a 12-well plate and blocked in IF blocking buffer: PBS with 5% normal goat serum and 0.5% Triton-X. A primary antibody solution comprised of 1:500 rabbit anti-Synaptophysin and 1:1000 mouse anti-SMI-312 in IF blocking buffer was applied onto the muscle sections and left on overnight at 4°C. Sections were then washed with PBS with 0.5% Triton-X, incubated with α -bungarotoxin and goat anti-rabbit and anti-mouse secondary antibodies conjugated to Alexa Fluor-488 (Invitrogen), and washed again. Sections were spread on slides and coverslips were attached using Prolong Gold Antifade Reagent (Life Technologies). Slides were examined using a Zeiss LSM 510 Meta confocal microscope.

Muscle Histology

Frozen quadriceps muscle was mounted using O.C.T. Compound and cut into 10 μ m cross-sections onto slides using a cryostat (Leica). For Hematoxylin and Eosin staining of muscle, sections were covered for 20 minutes with fixation buffer (4% Paraformaldehyde in 0.1M Phosphate Buffer, pH 7.4). Then sections were rinsed with distilled water, stained with Mayer's Hemalaun, rinsed again, and stained with Eosin. After a final rinse, samples were dehydrated in ethanol and xylene, and coverslips were applied.

For esterase staining, a staining solution was prepared containing 25% α -naphthyl acetate, 5% acetone, 0.1% Pararosaniline HCL, and 0.1% Sodium Nitrate in 0.2M Sodium Phosphate. The solution was applied to quadriceps sections for 5 minutes, after which sections were rinsed in running tap water for several minutes. Samples were then dehydrated in ethanol and xylene, and coverslips were applied. Esterase and H+E-stained sections were analyzed under light microscopy (Olympus).

Statistical Analysis

Data were analyzed using Microsoft Excel and GraphPad Prism software, with *P* values calculated using unpaired Student's *t* tests. *P* values less than 0.05 were considered significant. All quantitative values were reported as mean \pm standard deviation (SD).

RESULTS

S97 and W2 Transgenic Mice Expressed Human TDP-43 in Neuronal Tissues to Moderate and Comparable Levels

Given the line-to-line variability of transgenic mouse lines in general and of those lines generated using the Thy1.2 expression cassette in particular, it was important to characterize the human TDP-43 expression level and pattern in each line. To accomplish this, transgenic mice expressing human TDP-43^{G298S} from the newly generated line denoted S97 were compared to transgenic mice expressing human TDP-43^{Wild-Type} (W2), and to nontransgenic littermate controls (NT). Transgenic mice in lines S97 and W2 both expressed human TDP-43 in cortex, brain stem, and spinal cord, as detected on immunoblotting with a mouse monoclonal antibody specific for human TDP-43 (Figure 1). Furthermore, expression of human TDP-43 in S97 transgenic mice was confined to neuronal tissue and no expression could be detected in heart, muscle, or kidney tissue (Figure 2). This result supported the assertion that the Thy1.2 cassette drove expression mainly in neurons.

Densitometric quantification of several immunoblots showed that total (mouse plus human) TDP-43 levels in the cortex and spinal cords of both S97 and W2 transgenic mice were moderately elevated above the endogenous mouse TDP-43 level (Figure 4). Total TDP-43 levels in the cortexes of both S97 and W2 transgenic mice were close to 1.3 times the endogenous mouse TDP-43 level. Meanwhile, total TDP-43 levels in the spinal cords of both S97 and W2 transgenic mice were close to 1.6 times the endogenous mouse TDP-43 level. Fortuitously, it appeared that TDP-43 expression levels in S97 and W2 transgenic mice were very similar.

The pattern of human TDP-43 expression was also studied in S97 transgenic, W2 transgenic, and NT mice. Immunohistochemical staining of brain and spinal cord showed wide, robust neuronal expression of human TDP-43 in both S97 and W2 transgenic mice, with no unexpected areas of diminished expression (Figures 5 and 6). In sum, based on the TDP-43 expression level and pattern of transgenic mice from each line, the S97 and W2 lines are comparable.

Transgenic Mice Developed Muscle Weakness and Paralysis

In every litter of S97 or W2 mice, there were usually one or two small, dead transgenic pups by 3 weeks of age, but otherwise transgenic animals survived into adulthood. Many of the transgenic S97 and W2 mice developed abnormal hindlimb reflex by 1 month of age (Figure 7). By 2 months of age, transgenic S97 and W2 mice already had significantly shorter stride lengths than NT mice when forced to walk on a treadmill (Figure 10). Transgenic mice could not propel themselves forward sufficiently with normal strides, and instead were forced to take shorter, choppy strides. At 3-5 months of age, S97 and W2 mice were significantly weaker than their NT counterparts, unable to hang for 60 seconds upside-down on a metal grid (Figure 9). By 12 months of age, the weights of S97 and W2 transgenic males had plateaued such that they had significantly lower masses than their NT littermates (Figure 8).

Around 18 to 28 months of age, some transgenic S97 and W2 mice became paralyzed. Often the onset of paralysis was accompanied by a 10% or greater loss in weight. In one cohort of S97 transgenic males, four of twelve mice became paralyzed prior to death. In a cohort of W2 transgenic males, four of eight mice became paralyzed

prior to death. The rest died presumably prior to the age when they would have developed paralysis. When analyzed on a Kaplan-Meier survival curve, the lifespan of S97 and W2 transgenic mice is significantly shorter than the lifespan of NT littermates (Figure 11).

No Cytoplasmic Inclusions were Observed in Transgenic Mice

Cytoplasmic mislocalization of TDP-43 and cytoplasmic inclusions containing TDP-43 were prominently seen in ALS patient samples (Neumann et al., 2006), and rarely seen in TDP-43 transgenic mouse models (Tsao et al., 2012; Arnold et al., 2013). In S97 and W2 transgenic mice, both Human TDP-43 and Mouse TDP-43 remained confined to the nucleus of cortical and spinal cord cells. No cytoplasmic inclusions containing TDP-43, or nuclear clearing of TDP-43, were observed (Figures 12, 13, 14, and 15).

Transgenic Mice Lost Many L3 Large Motor Axons by 2 Months of Age, and Continued to Lose More

The lumbar L3 ventral roots of NT mice and S97 and W2 transgenic mice were evaluated at 2 months, 12 months, and End Stage using Toluene-stained epon thick sections. In L3 roots from NT mice, there is a bimodal distribution of axon diameters (Figure 18), with smaller fibers (Feret diameter $<4.5\mu\text{m}$) likely representing the axons of γ -motor neurons and larger fibers (Feret diameter $\geq 4.5\mu\text{m}$) likely representing the axons of α -motor neurons responsible for voluntary muscle contraction. As NT animals age to 12 months, the diameters of the larger fibers in particular increase, with increasing animal

size and muscle tone. Near the end of life, the distribution of axon diameters in NT L3 roots is similar to the distribution earlier in life at 2 months, as NT animals aged close to 2 years have experienced normal age-related declines in size (Figure 8) and muscle tone.

Even by the age of 2 months, S97 and W2 transgenics already have many fewer L3 large motor axons (Ferret diameter $\geq 4.5\mu\text{m}$) compared to NT mice (Figures 16, 18, and 20). Perhaps the transgenic mice never developed these missing large axons, or the transgenics lost them at some point earlier than 2 months of age. In fact, at 2 months of age the number of “missing” large axons in the L3 ventral roots of S97 and W2 transgenic mice is already greater than 200 fibers (Figure 21). This number increases to greater than 300 lost large motor axons when comparing S97 and W2 transgenic mice to NT mice at 12 months of age. This indicates continued degeneration of large motor axons, which is shown histologically by the presence of vacuoles (Figure 17). This degeneration appears to plateau, with transgenic mice at End Stage still retaining some large motor axons (Figure 20).

Also of note is the observation that many of the S97 and W2 transgenic mice had L3 dorsal roots that were noticeably smaller than similar roots from NT mice (Figure 22). This could be an indication of concurrent sensory deficits present in the S97 and W2 transgenic mice, which aligns with the observations made by several groups that ALS may involve the sensory nervous system in some patients (Theys et al., 1999; Pugdahl et al., 2007).

Neuromuscular Junctions were Denervated in Transgenic Mice

In order to visualize the downstream effects of ventral root large fiber degeneration, neuromuscular junctions were analyzed in gastrocnemius muscles from S97 transgenic, W2 transgenic, and NT 2- and 12-month-old and end-stage male mice. Many junctions in 2-month-old S97 and W2 transgenic mice appeared well-innervated, while many denervated junctions could be found in 12-month-old S97 and W2 transgenic mice (Figure 23). Muscle in end-stage S97 and W2 transgenic mice degenerated to the point where it was difficult even to find intact α -bungarotoxin-stained motor end plates. The effects of long-term denervation of muscle have caused the loss of motor end plates, likely resulting in the paralytic phenotype observed in these End-Stage transgenic mice.

Muscle Degeneration in Transgenic Mice

Muscle pathology was observed through analysis of quadriceps muscles from S97 transgenic, W2 transgenic, and NT 2- and 12-month-old and end-stage male mice. The quadriceps muscle analysis was an appropriate choice to pair with the L3 ventral root analysis, because the motor neurons innervating the quadriceps muscle lie in the L1 to L3 spinal cord region in mice (McHanwell and Biscoe, 1981). Given how many large motor axons had already been lost from L3 ventral roots of S97 and W2 transgenics at 2 months of age, the muscles from 2-month-old transgenic animals looked remarkably intact (Figure 24). Hematoxylin and eosin staining showed muscle fibers that appear mostly normal in size and shape compared with muscle fibers in NT mouse quadriceps. In addition, esterase staining, which is darker in denervated fibers, revealed some

denervation in 2 month transgenic mouse muscle but the checkerboard pattern of different fiber types remained relatively intact compared with NT mouse quadriceps.

By 12 months of age, the fiber architecture of S97 and W2 transgenic mouse muscle was significantly altered compared to that of NT mouse muscle. H+E staining showed disorganization of muscle fibers and small, angulated fibers. In addition, infiltration of the muscle by fibrous tissue could be observed. These findings were typical of long-term denervation of muscle (Carlson et al., 2002). Esterase staining in the quadriceps of 12-month-old transgenic mice showed increased denervation and fiber type grouping, with large regions of muscle that had lost the normal checkerboard pattern of esterase staining. The disruption of normal muscle architecture was even more severe in muscle from End Stage transgenic S97 and W2 mice.

DISCUSSION

From the phenotypes described in published TDP-43 mouse models as well as the results described here, we can infer that there are two stages of TDP-43 toxicity in overexpression models. First, there is significant toxicity very early in life, and transgenic animals at just weeks old are often smaller, and have abnormal hind limb reflexes or tremor when compared with nontransgenic littermates (Wegorzewska et al., 2009; Stallings et al., 2010; Xu et al., 2010; Wils et al., 2010; Shan et al., 2010; Zhou et al., 2010, Janssens et al., 2013). In some mouse lines with very high TDP-43 levels, none of the transgenic animals can survive this early stage of toxicity (Shan et al., 2010; Stallings et al., 2010; Janssens et al., 2013). In lines with lower TDP-43 levels, however, transgenic mice can survive for a year or longer, continuing to grow even if they are

weaker compared to their littermates (Wils et al. 2010; Tsai et al., 2010; Igaz et al., 2011; Swarup et al., 2011; Arnold et al., 2013; Stribl et al., 2014). These mice may eventually experience the second, degenerative, phase of TDP-43 toxicity. This phase is characterized by gait abnormalities and muscle weakness potentially leading to an end-stage paralysis, and better represents what we expect to happen in a model of ALS.

The creation and characterization of the transgenic mouse lines S97 and W2 fills a void in the spectrum of transgenic TDP-43 mouse models (Figure 25). Transgenic mice in these two lines do suffer the early toxicity seen in mice of many other transgenic TDP-43 lines. To wit, early in life, S97 and W2 transgenic mice show hind limb claspings, gait abnormalities with shorter forced stride lengths, loss of large motor axons in the L3 ventral roots, and diminished size of L3 dorsal roots. However, many S97 and W2 transgenic mice also survive to adulthood, gain weight appropriately before plateauing, exhibit a progressive loss of strength in the hanging wire tests, and lose more large motor axons in their adult life. Also, S97 and W2 transgenic mice display adult-onset muscle degeneration and neuromuscular junction and motor end-plate abnormalities. Significantly, a percentage of S97 and W2 transgenic mice progress to paralysis late in life. The S97 and W2 lines represent the first transgenic TDP-43 mouse lines with mice that exhibit motor neuron degeneration leading to paralysis in late adulthood. As such, we believe that these mouse lines are a best mimic of human disease amongst TDP-43 transgenic mouse lines yet reported.

Additionally, given that the W2 and S97 lines are so well-matched in expression level and pattern, we can report that the ALS-Linked mutation G298S does not appear to cause any additional effects beyond the overexpression effect of TDP-43. W2 and S97

lines were similar phenotypically and histologically. If anything, W2 transgenic mice trended towards being more likely to get paralyzed, and being more likely to die early. Genetic evidence suggested the possibility that disruption of autoregulation of TDP-43 in ALS by mutations in the 3'UTR of its own mRNA could lead to modest elevation of TDP-43 (Gitcho et al., 2009). That modest accumulation of TDP-43 in neurons of W2 or S97 line is sufficient to cause motor neuron disease would strongly support the idea that disruption of TDP-43 autoregulation to modestly elevate its levels is one pathogenic mechanism underlying neurodegeneration in ALS. Reports in the literature on the mutation effect are mixed, with some groups maintaining that there is a mutation effect on neurodegeneration in TDP-43 mouse models, with the G348C mutation (Swarup et al., 2011), the Q331K mutation (Arnold et al., 2013), the M337V mutation (Janssens et al., 2013), or the A315T mutation (Stribl et al., 2014). Other groups, however, have seen no phenotypic differences between expressing wild-type human TDP-43 and human TDP-43^{M337V} (Xu et al., 2010; Xu et al., 2011).

Unfortunately, the creation of these mouse lines still cannot answer the question of whether neuronal toxicity is caused by expression the toxic human TDP-43 itself, or by nonfunctional human TDP-43 driving down the levels of functional mouse TDP-43 by autoregulation (Ayala et al., 2011; Igaz et al., 2010; Polymenidou et al., 2011). Evidence from mouse TDP-43 rescue experiments suggests that the toxic mechanism is accumulation of human TDP-43 (Xu et al., 2013). Nevertheless, lines of mice expressing modest levels of TDP-43 exhibiting age-dependent motor neuron disease will be useful to further clarify disease mechanisms and for testing therapeutic strategies to attenuate neurodegeneration in ALS.

**CHAPTER 3: IDENTIFICATION OF PATHWAYS IMPACTED BY MODEST
INCREASE OF TDP-43 IN NEURONS: TRANSCRIPTOME ANALYSIS OF
SPINAL CORDS FROM S97 AND W2 MICE**

INTRODUCTION

The discoveries that RNA binding proteins, including TDP-43, FUS/TLS, and MATR3, were involved in the pathogenesis of ALS/FTLD-TDP inspired the idea that the disease was one of altered RNA metabolism (Lagier-Tourenne and Cleveland, 2009). The notion that altered RNA metabolism played a crucial role in ALS/FTLD was further emphasized by the discovery that a hexanucleotide repeat expansion in an intron of a previously uncharacterized gene, termed *C9ORF72*, was the cause of a major proportion of cases (DeJesus-Hernandez et al, 2011; Renton et al, 2011). Other studies demonstrated through immunoprecipitation and mass spectrometry that TDP-43 interacted with RNA splicing and translation proteins (Freibaum et al., 2010). In our lab, Shan and Chiang showed that TDP-43 regulates the formation and distribution of Survival Motor Neuron (SMN)-containing Gemini of coiled bodies (GEMs), machinery that is required for the assembly of snRNPs involved in RNA splicing (Shan et al., 2010).

Several studies aimed to identify the transcripts that were bound by TDP-43 and were altered by overexpression or knockdown of TDP-43 (Polymenidou et al., 2011; Tollervey et al., 2011; Sephton et al., 2011; Xiao et al., 2011; Colombrita et al., 2012; Narayanan et al., 2013). These studies were based on using cross-linking immunoprecipitation to isolate TDP-43 in complex with RNA (Buratti et al., 2013). The RNA was then released, and a cDNA library was generated and studied on microarrays or using deep sequencing. TDP-43-bound transcripts were thus identified in adult mouse brain (Polymenidou et al., 2011; Narayanan et al., 2013), NSC-34 hybrid mouse motor neuron-like cells (Sephton et al., 2011; Colombrita et al., 2012); SH-SY5Y human

neuroblastoma cells (Tollervey et al., 2011; Xiao et al., 2011), and FTLD brains and human embryonic stem cells (Tollervey et al., 2011).

To aid in the discovery of genes that could promote neurodegeneration when TDP-43 is modestly elevated in neurons in the S97 and W2 transgenic TDP-43 mice, we focused on using an RNA sequencing approach. We chose to study the spinal cord mRNA of young mice, at 6 weeks of age, in an attempt to find transcriptional changes during the early stages of neurodegeneration. For RNA sequencing, extracted RNA was used to generate a library comprised of cDNA fragments with sequencing adapters. These fragments were sequenced, yielding many reads. Transcripts that, prior to fragmentation, were longer or more prevalent were read more times during the sequencing process. Mapping and quantification of the reads would allow us to generate a transcriptome-wide view of expression level and splicing differences between S97 transgenic, W2 transgenic, and NT mice.

MATERIALS AND METHODS

RNA Sequencing

The ventral halves of spinal cords were dissected from freshly euthanized 6-week-old male mice, and transferred immediately into RNAlater storage reagent (Life Technologies). Two W2 transgenic animals and one NT littermate control were dissected. Similarly, two S97 transgenic animals and one NT littermate control were dissected. Spinal cord tissue was processed using the RNeasy Mini Kit (Qiagen) to extract total RNA. RNA concentration was measured on a NanoDrop Spectrophotometer and greater than 1 µg of total RNA for each sample was submitted to the Genetic Resources Core

Facility at the Johns Hopkins School of Medicine. There, each RNA sample was fragmented and paired-end cDNA libraries were created. Each library was then sequenced with 100 base pair paired-end reads on an Illumina HiSeq system.

Data were returned from the sequencer in the form of .fastq files. These files were “groomed,” or converted, into .fastqsanger files using Galaxy (Blankenberg et al., 2010). The Tophat program on Galaxy was then used to map sequencing reads onto the mouse (mm9) genome. Tophat files were used in the Cufflinks/Cuffdiff program in Galaxy to analyze differential expression, or were converted to .bigwig files for visualization on the UCSC Genome Browser. For determination of human *TARDBP* expression level, .fastqsanger data was mapped onto the human (hg19) genome and analyzed using the Cufflinks program on Galaxy.

RESULTS

S97 and W2 Transgenic Mice Had Reduced Mouse *TARDBP* Levels

The mRNA levels of mouse and human *TARDBP* were determined in 6-week-old mouse spinal cords using RNA sequencing data processed with Cufflinks/Cuffdiff (Figure 26). NT mice expressed no human *TARDBP* mRNA, as expected. In both S97 and W2 transgenic mice, total (mouse + human) *TARDBP* mRNA levels were in the range of 1.7 to 1.8 times the total *TARDBP* mRNA levels in NT mice. This result correlated well with the total TDP-43 levels in the spinal cord, which in transgenic S97 and W2 mice were about 1.6 times the total TDP-43 level in NT mice (Figure 4). Also, as expected due to TDP-43 autoregulation, the expression levels of mouse *TARDBP*

(*mTARDBP*) mRNA in transgenic S97 and W2 animals were diminished compared to the level in NT mice.

An Alternatively-Spliced Form of *ARHGAP44* was Identified in Transgenic Mice

Cufflinks/Cuffdiff analysis of RNA sequencing data returned a large number of transcripts with significantly higher or lower expression levels in transgenic S97 and W2 mice than in NT mice. Meanwhile, the number of transcripts significantly different between S97 and W2 mice was much smaller (Figure 27). This result demonstrated that the transgenic S97 and W2 transcriptomes were relatively similar, while each transgenic transcriptome was markedly different from the NT transcriptome.

One of the transcripts whose expression level was most different, when comparing S97 and W2 transgenics to NT mice, was *ARHGAP44* (Figures 28, 29). Mapping RNA sequencing data into the UCSC Genome Browser demonstrated that one small, 52-base pair exon of *ARHGAP44* is more frequently spliced out in the transgenic S97 and W2 mouse spinal cords (Figure 30). Information from UCSC and NCBI revealed that *ARHGAP44* had two transcript variants. Variant 1 (NM_001099288) excluded the small exon and encoded an 814-amino acid isoform. Meanwhile, Variant 2 (NM_175003) included the small exon, which had an in-frame stop codon, and encoded a 764-amino acid isoform with a truncated C-terminal domain. Transcript variant 2, the longer mRNA encoding the shorter isoform, is the one predominantly expressed in the spinal cords of 6-week-old NT mice. Meanwhile, transcript variant 1, the shorter mRNA encoding the longer isoform, is the one predominantly expressed in the spinal cords of the transgenic S97 and W2 mice.

To test whether this was the case, an antibody against ArhGAP44 (also known as Rich2) was used to stain lysates of S97 transgenic and NT spinal cord. At 2-, 12-, and 24-months of age, transgenic S97 mice expressed a larger ArhGAP44 isoform than the isoform expressed in NT mice (Figure 31).

DISCUSSION

Deep sequencing experiments can be complex and expensive, demanding input RNA of high concentration and purity and producing output data that requires nuanced analysis (Buratti et al., 2013; Pollier et al., 2013). The validity of the RNA sequencing experiment reported here was demonstrated in two ways. First, the *mTARDBP* transcript level in transgenic S97 and W2 mouse spinal cords was lower than the transcript level in the spinal cords of NT mice. This result was consistent with what was expected due to TDP-43 autoregulation, and what had been seen in other transgenic TDP-43 mouse models (Igaz et al., 2010; Xu et al., 2011; Arnold et al., 2013). Secondly, *ARHGAP44* transcript variant 1 was shown in the RNA data to be elevated in the S97 and W2 transgenic mice, and indeed the larger ArhGAP44 isoform is present in the transgenic spinal cords immunoblots.

This RNA sequencing study was designed to examine the global effect of elevated TDP-43 levels on the transcriptomes of 6-week-old mouse spinal cords. Thus this study could not identify what transcripts were directly interacting with TDP-43. Similarly, this study could not determine whether a transcript expression level difference or a splicing alteration was a cause of or a result of TDP-43 toxicity. For example, the expression of

certain genes could be altered in the TDP-43 transgenic mice as an inflammatory response to toxicity.

Nevertheless, ArhGAP44 is an intriguing protein to examine in future studies. ArhGAP44, also known as Rich2 (RhoGAP Interacting with Cdc-42-interacting Protein 4 Homolog 2), was identified in 2001 as GTPase Activating Protein acting on the Rho GTPases Rac1 and Cdc42 (Richnau and Aspenstrom, 2001). The reported functions of ArhGAP44 include interacting with CD317 to maintain actin cytoskeleton organization in epithelial cells (Rollason et al., 2009), interacting with Shank3 to promote long-term potentiation (Raynaud et al., 2013), and interacting with Rac1 to promote dendritic spine development (Raynaud et al., 2014) or inhibition (Galic et al., 2014). Data from the GNF Expression Atlas 2 shows that *ArhGAP44* is highly expressed in brain and spinal cord tissue, and not in immune tissue (Su et al., 2004). *ArhGAP44* is not found in any of the previously reported datasets of transcripts to which TDP-43 directly binds (Polymenidou et al., 2011; Tollervey et al., 2011; Sephton et al., 2011; Xiao et al., 2011; Colombrita et al., 2012; Narayanan et al., 2013). However, one group reports TDP-43 interaction with *ArhGAP12* (Xiao et al., 2011), another reports TDP-43 binding to *ArhGAP8* and *-23* (Colombrita et al., 2012), and yet another reports TDP-43 binding to *ArhGAP5*, *-6*, *-20*, *-21*, and *-29* (Narayanan et al., 2013). Given TDP-43 binding to these related proteins, as well as the lack of overlap in the results these studies, it is not hard to imagine that TDP-43 may interact directly with the *ArhGAP44* transcript to mediate its alternative splicing. If this is the case, the biologic relevance of the different isoforms would be interesting to uncover. Of note, human ArhGAP44 also has two reported isoforms, at 818-amino acids and 768-amino acids (UniProt, 2015). Whether these different isoforms hold relevance to

TDP-43 proteinopathy or neurodegeneration remains to be discovered. Finally, not within the scope of this work, future efforts to examine other targets from our transcriptome analysis of mice with modest accumulation of TDP-43 may shed light regarding the mechanism whereby increase in TDP-43 promotes neurodegeneration in ALS.

CHAPTER 4: CONCLUDING REMARKS

Amyotrophic Lateral Sclerosis was first described over 140 years ago, and remains one of the most devastating human diseases. It has a rapid, relentlessly progressive nature, often taking people in mid-life who had appeared perfectly healthy from minor weakness to the wheelchair and then to the ventilator in just a couple of years. No disease-modifying therapies are available, and the gold standard drug therapy, Riluzole, may only prolong survival by months (Ludolph and Jesse, 2009). Thousands of people will be diagnosed with ALS in the United States this year, and for them, we have no good answers.

Nevertheless, we do know much more about ALS than we did just a decade ago. Genetic and pathologic studies using patient samples have allowed a rethinking of clinical classifications. Whereas not long ago ALS and FTLN were thought of as separate diseases, they are now believed to occupy the same disease spectrum. Also, with the knowledge that we now have about the genetic basis of ALS, it is conceptually possible to separate the disease into variants and to personalize care to patients with *SOD1* mutations, or with *TARDBP* mutations, or with *C9ORF72* expansion, or with a number of other gene differences.

One such variant found in the last few years was ALS/FTLN-TDP with 3'UTR *TARDBP* mutations. Patients with this disease entity had moderately elevated levels of *TARDBP*, possibly because the mutation compromised the ability of TDP-43 to downregulate its own transcript. Whether the modest increase in TDP-43 seen in these patients could be sufficient to cause motor neuron disease was an open question. We aimed to answer that question, by creating and characterizing lines of transgenic mice that accumulated modest levels of TDP-43 in the nervous system. One of these lines,

S97, expressed *TARDBP* carrying the ALS associated missense mutation (corresponding to the mutant G298S protein), whereas the other line, W2, expressed wild-type human *TARDBP*.

There are many features of the S97 and W2 lines that make them good models for ALS. Most of the transgenic mice survive to adulthood, gain weight appropriately before plateauing, exhibit a progressive loss of strength, and lose large motor axons in their adult life. Also, S97 and W2 transgenic mice display adult-onset muscle degeneration and neuromuscular junction and motor end-plate abnormalities, progressing to paralysis late in life. The S97 and W2 lines are the first transgenic TDP-43 lines that develop motor neuron degeneration leading to paralysis in late adulthood. These lines demonstrate that a moderate increase in TDP-43 is sufficient to cause an ALS-like phenotype.

Of course, there are aspects of the S97 and W2 lines that do not mimic ALS. Significant early-phase TDP-43 toxicity occurs, and S97 and W2 transgenic mice develop abnormal hind-limb reflexes and abnormal gaits early in life. Transgenic mice also lose a high percentage of the large motor axons in the L3 ventral roots by the time they are 2 months old. This does not seem to correlate with clinical ALS, in which patients are seemingly normal prior to developing symptoms. However, it is possible that ALS patients start losing motor neurons many years prior to the onset of symptoms, and only develop weakness when they have lost their ability to compensate. After all, ALS/FTLD-TDP patients with mutations in *TARDBP* or other genetic abnormalities carry those abnormalities throughout their lives. Perhaps the injury that eventually leads to disease begins much earlier, in childhood or before (Van Zundert et al., 2012).

One other advantage of working with the S97 and W2 transgenic mouse lines is that the level and pattern of TDP-43 expression is well matched. If there were any additional effects of the G298S mutation, we would have expected to find them. However, the S97 and W2 transgenic mice have such similar phenotypes, pathology, and RNA transcript profiles that it is likely the G298S mutation itself has no effect in these mice. As such, the S97 line is best viewed as an overexpression model rather than a mutation model.

As models of modest TDP-43 overexpression, these transgenic mouse lines will be useful platforms for further inquiry into the mechanisms of neurodegeneration. We have begun this work already with our RNA sequencing experiments, identifying, in *ARHGAP44*, a promising gene for future studies. In addition, these mouse lines can be platforms for the testing of new therapeutics. Perhaps compounds that can lower the amount of total TDP-43 could prevent the motor degeneration in these mice, and be useful in the future in humans.

FIGURES



Figure 1: Expression construct used to generate mice. The human *TARDBP* cDNA was cloned downstream of the Thy1.2 Essential Promoter.

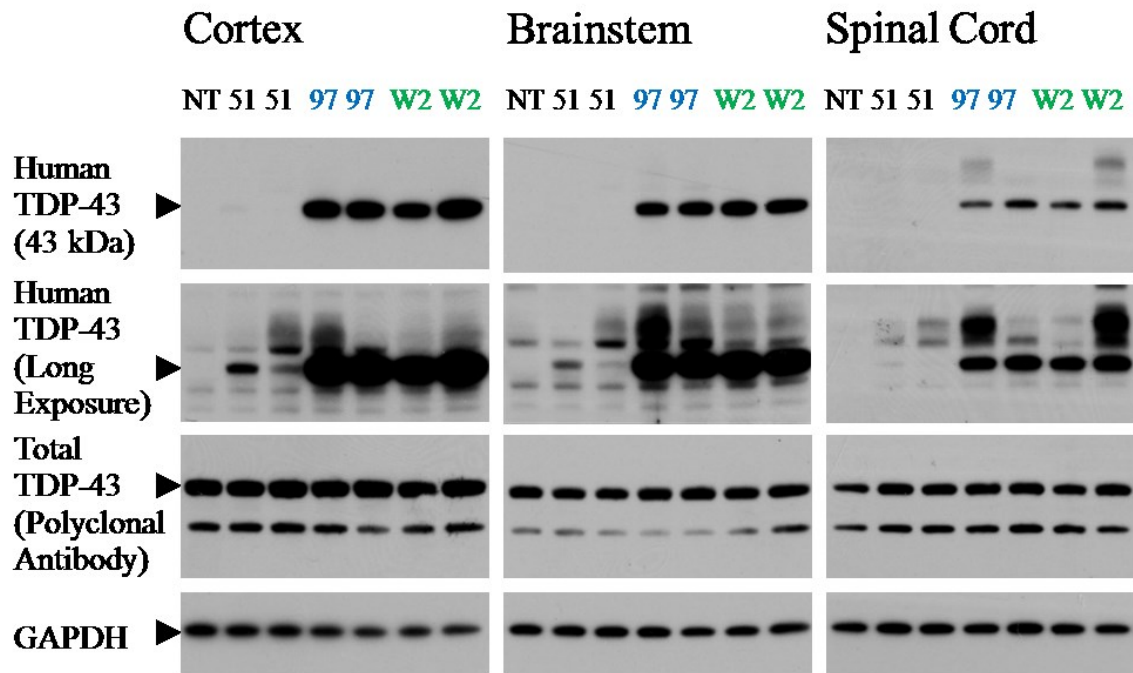


Figure 2: Western blots showing protein expression levels in various neural tissues from 2-month-old male Nontransgenic (NT), S51 transgenic, S97 transgenic, and W2 transgenic mice. Human TDP-43 is clearly detected in S97 transgenic and W2 transgenic tissue extracts using a mouse monoclonal antibody specific for human TDP-43 (Novus). Human TDP-43 is more difficult to detect in S51 samples, and staining can only be seen on long exposures. A rabbit polyclonal antibody, detecting total (mouse + human) TDP-43, reveals strong bands in all lanes. Staining with a GAPDH antibody is used to show even loading.

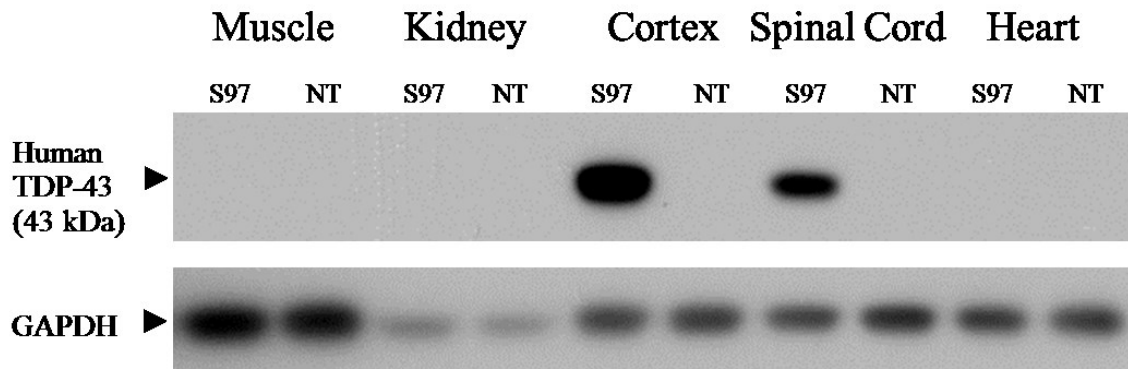


Figure 3: Western blot showing human TDP-43 expression in 2-month-old male S97 transgenic and NT mice. Using a mouse monoclonal antibody specific for human TDP-43 (Novus), protein is clearly detected in the neural tissues Cortex and Spinal Cord, but is absent in other tissues like Muscle, Kidney, or Heart. Staining with a GAPDH antibody is used to show even loading within each set of tissues.

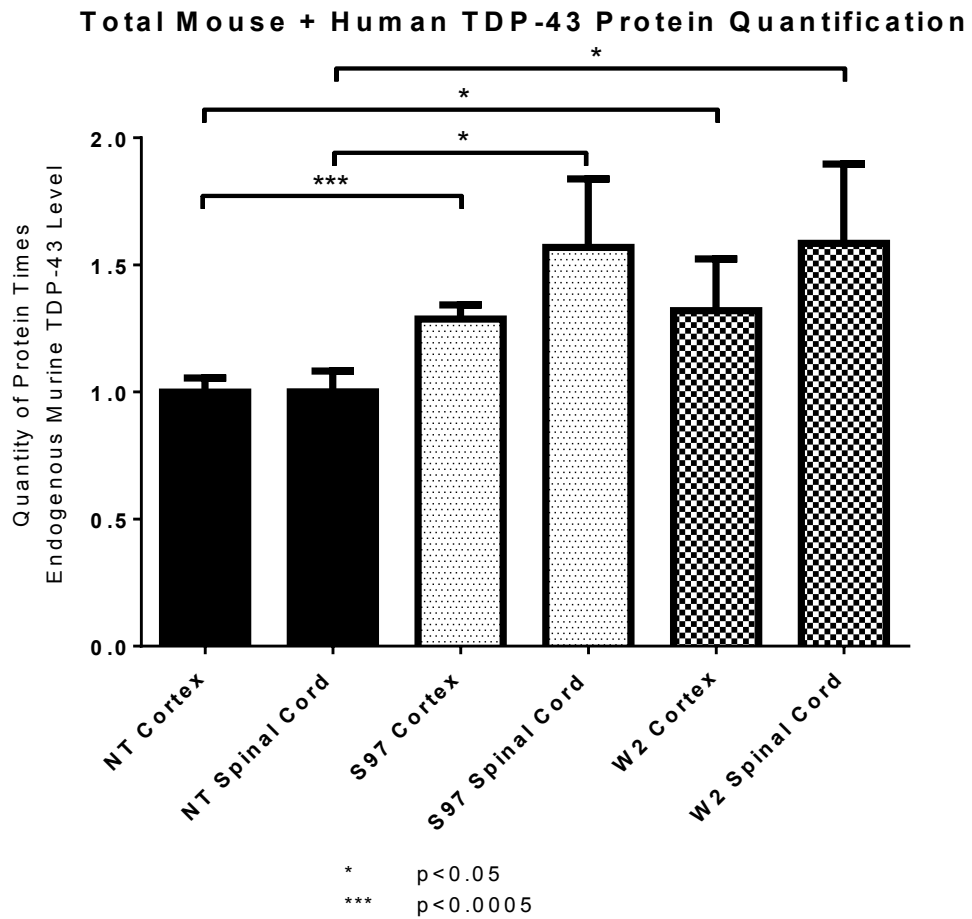
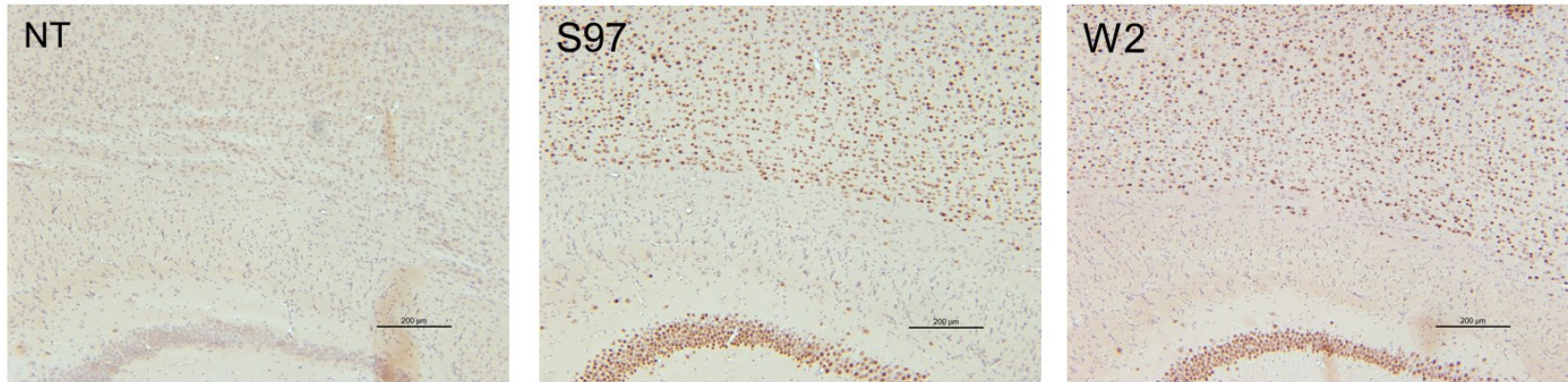
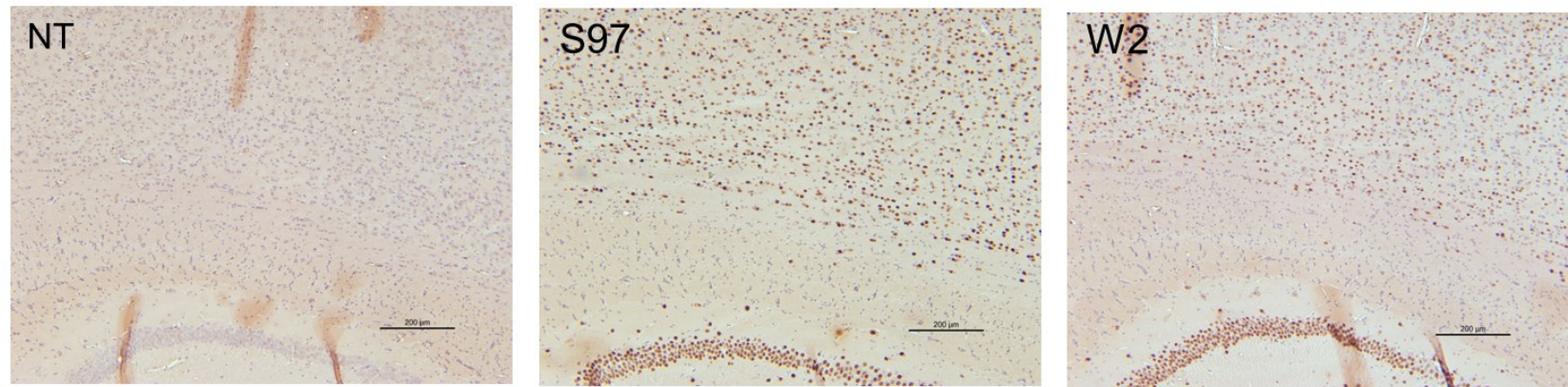


Figure 4: TDP-43 protein levels in 2-month-old male NT, S97 transgenic, and W2 transgenic animals. Densitometric analysis was performed using a rabbit antibody detecting total (mouse and human) TDP-43. Nontransgenic animals, n=3, S97 transgenic animals, n=4, W2 transgenic animals, n=4.

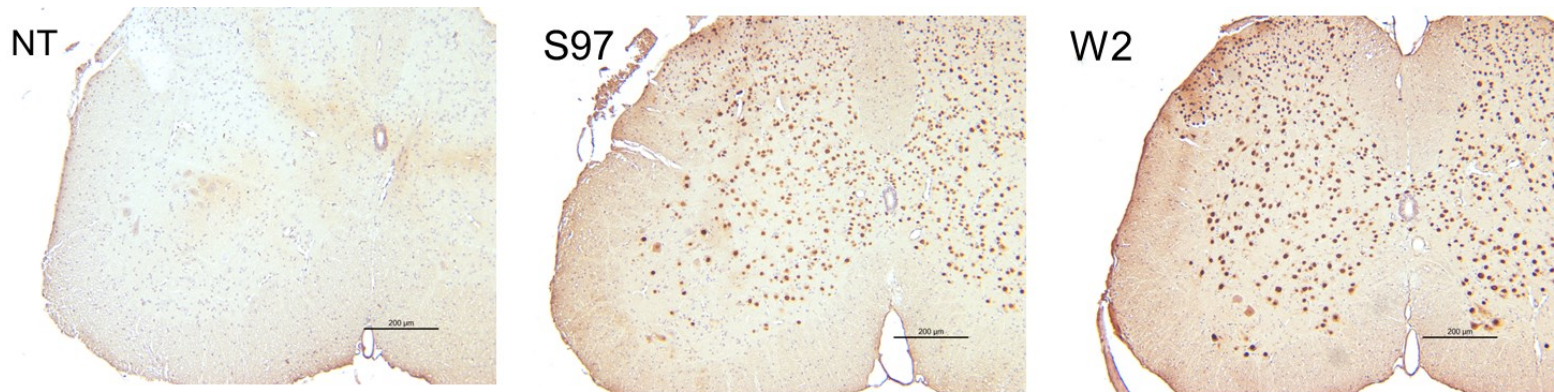


2mo, Novus mouse anti-human TDP-43

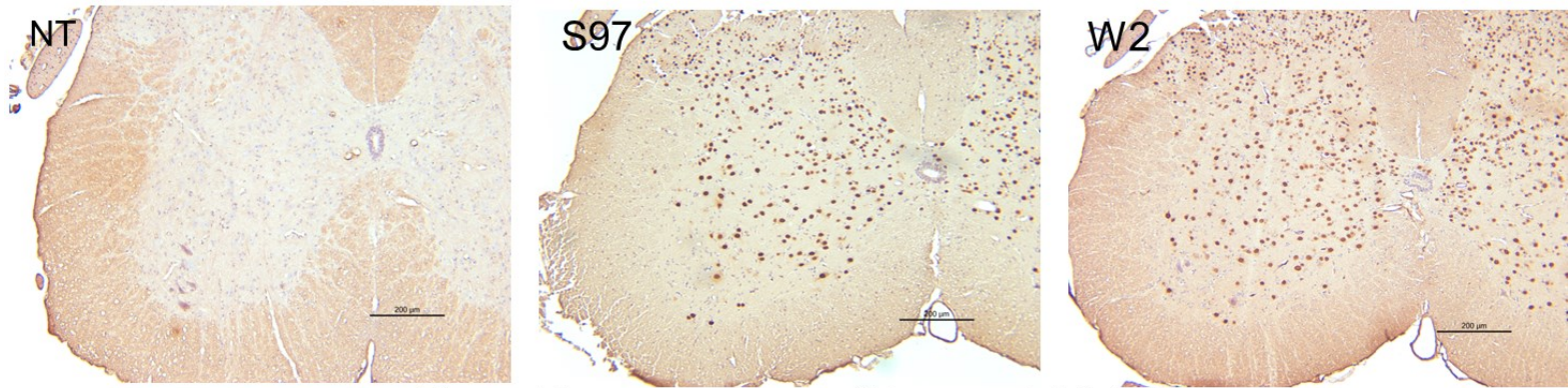


12mo, Novus mouse anti-human TDP-43

Figure 5: Human TDP-43 expression in brain sections of 2- and 12-month-old male Nontransgenic (NT), S97 transgenic, and W2 transgenic mice, as detected by a mouse antibody specific for human TDP-43 (Novus, dark brown stain). Blue hemalum counterstain.



2mo, Novus mouse anti-human TDP-43



12mo, Novus mouse anti-human TDP-43

Figure 6: Human TDP-43 expression in spinal cord sections of 2- and 12-month-old male Nontransgenic (NT), S97 transgenic, and W2 transgenic mice, as detected by a mouse antibody specific for human TDP-43 (Novus, dark brown stain). Blue hemalum counterstain.

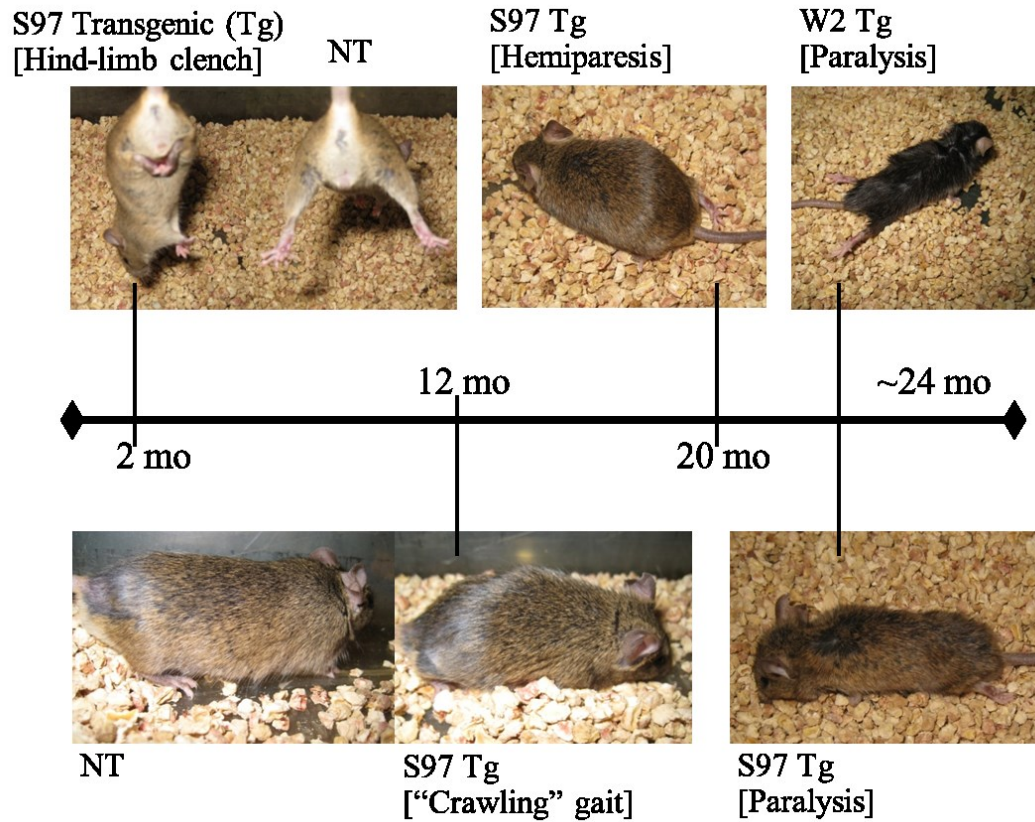


Figure 7: These images show mice in lines S97 and W2. Mice in both lines develop an abnormal hind-limb reflex (clenching) by 1 month, which continues throughout their lifespan. A “crawling” or “swimming” gait can be noticed at around 1 year. Mice in both lines may develop hemiparesis as early as 18-20 months, reaching end-stage beginning at 20-28 months.

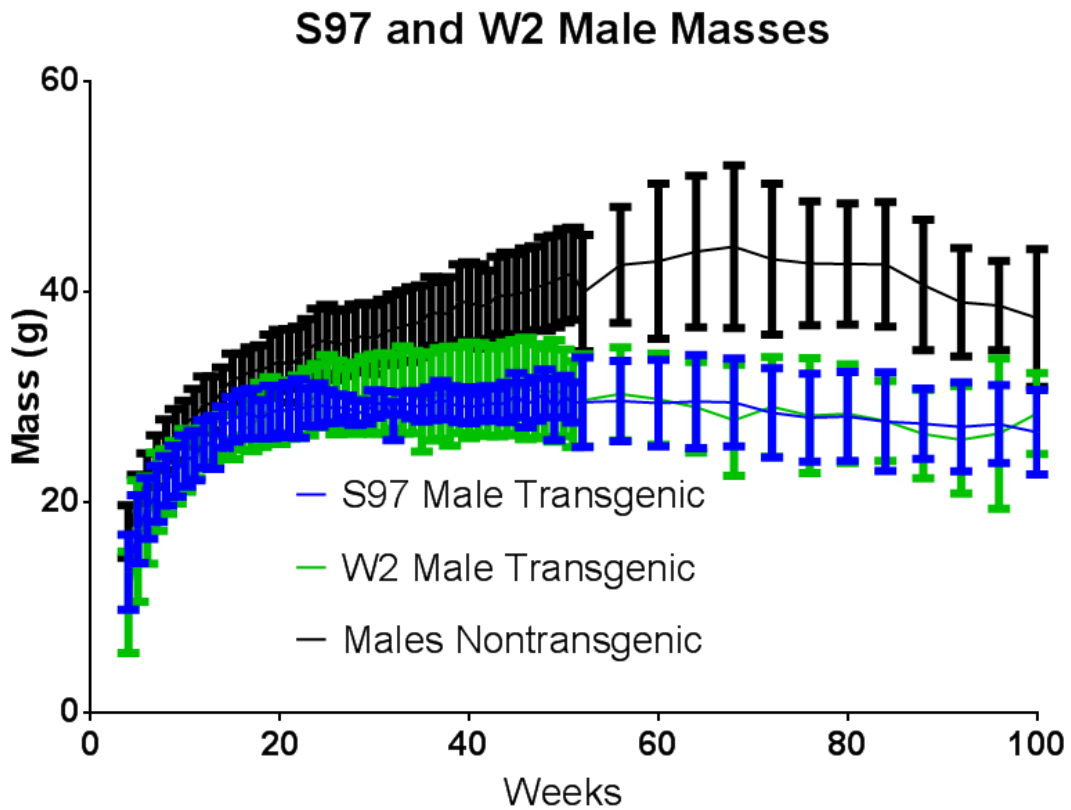


Figure 8: Mass data for male mice in the F3, F4, and F5 generations. The masses of transgenic mice plateau early and, as the animals age, become significantly lower than the masses of nontransgenic littermates. S97 transgenic, $n=33$, W2 transgenic, $n=21$, Nontransgenic, $n=44$. Error bars represent standard deviations.

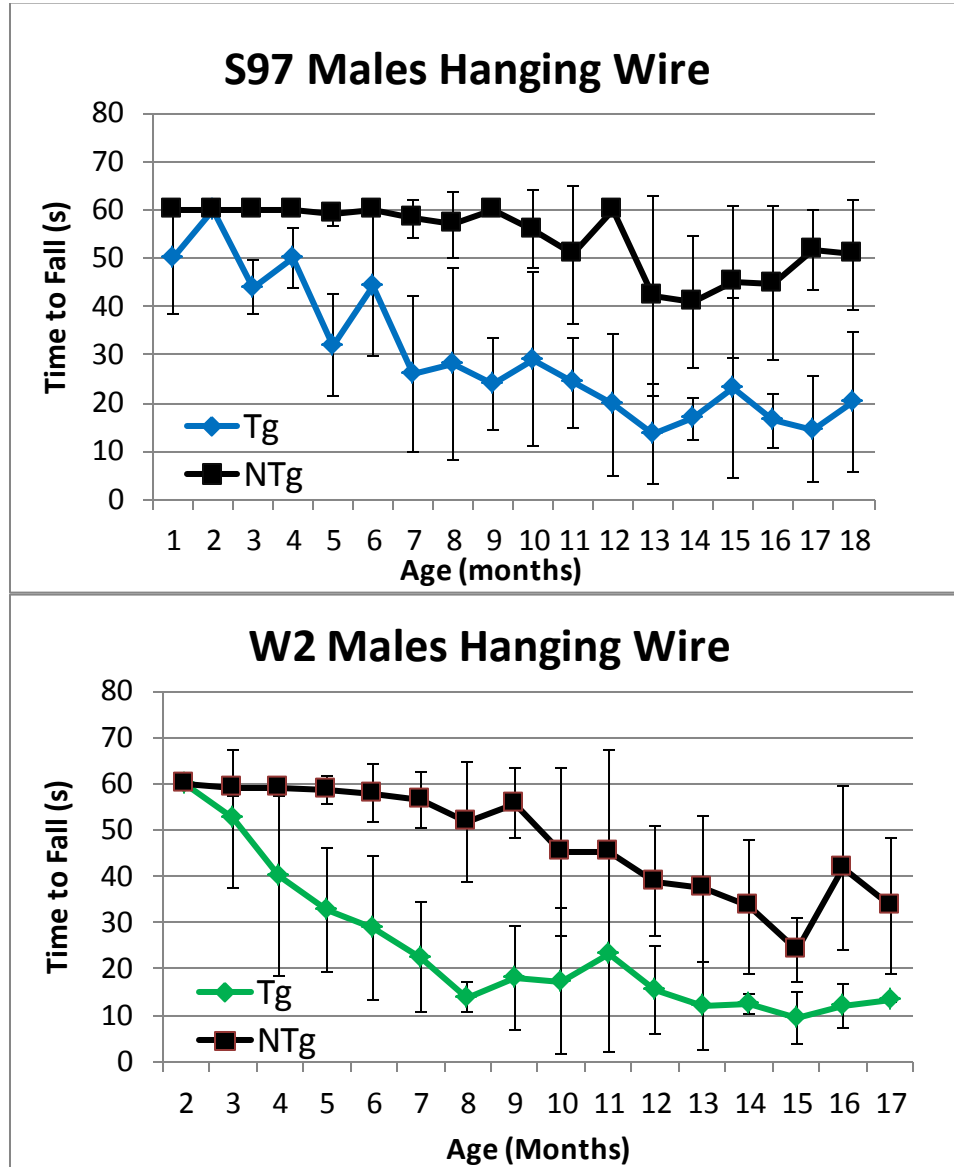


Figure 9: Testing the ability of S97 transgenic, W2 transgenic, and Nontransgenic (NTg) male mice (F5 generation) to hang upside-down on a wire grid for a maximum of 60 seconds. This test reveals significant early weakness in S97 transgenic mice compared to NTg littermate controls starting at 3 months, and in W2 transgenic mice compared to NTg littermate controls starting at 5 months. S97 Tg, n=14, NTg, n=14, W2 Tg, n=16, NTg, n=18. Error bars represent standard deviations.

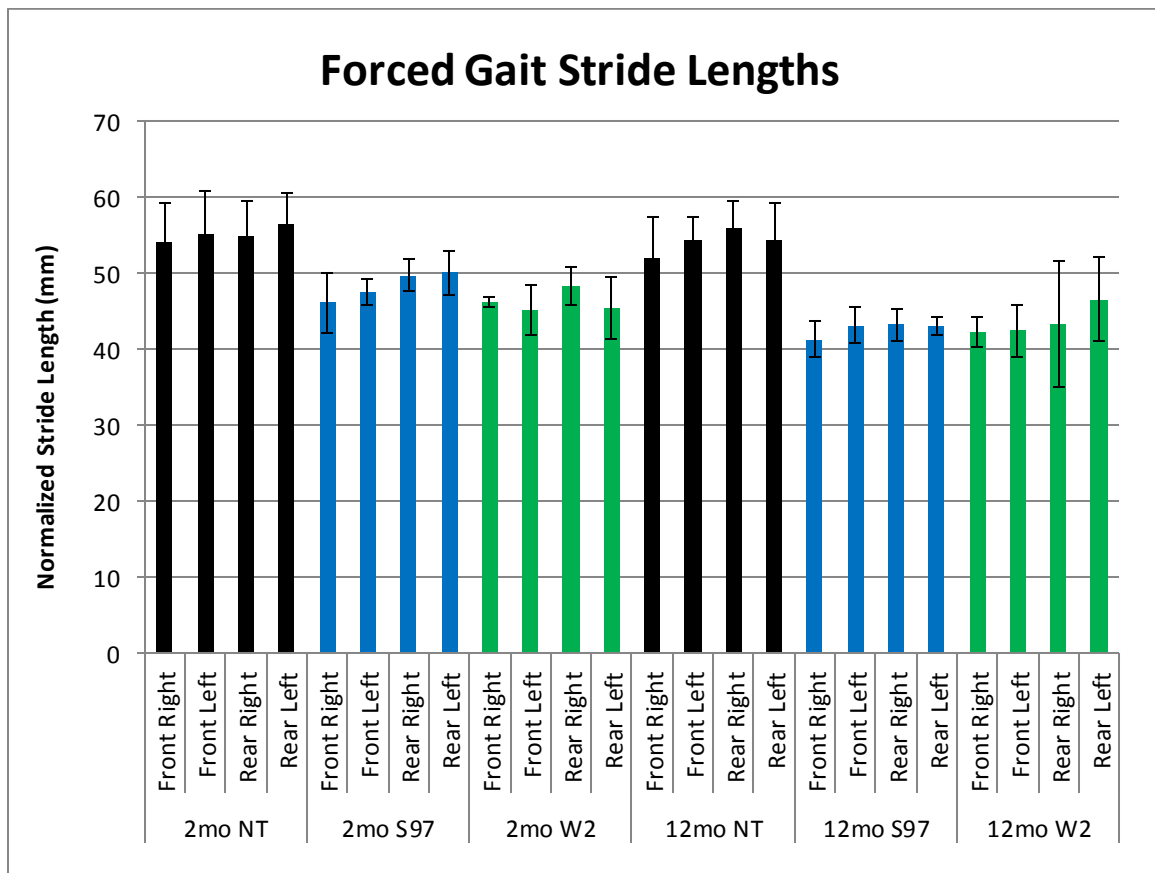
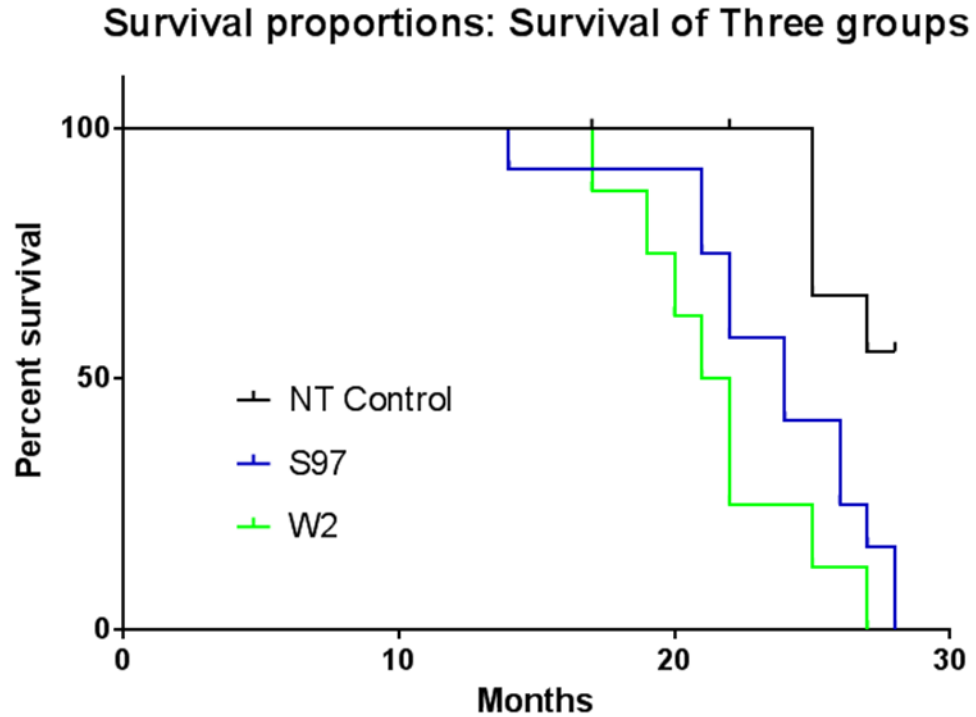
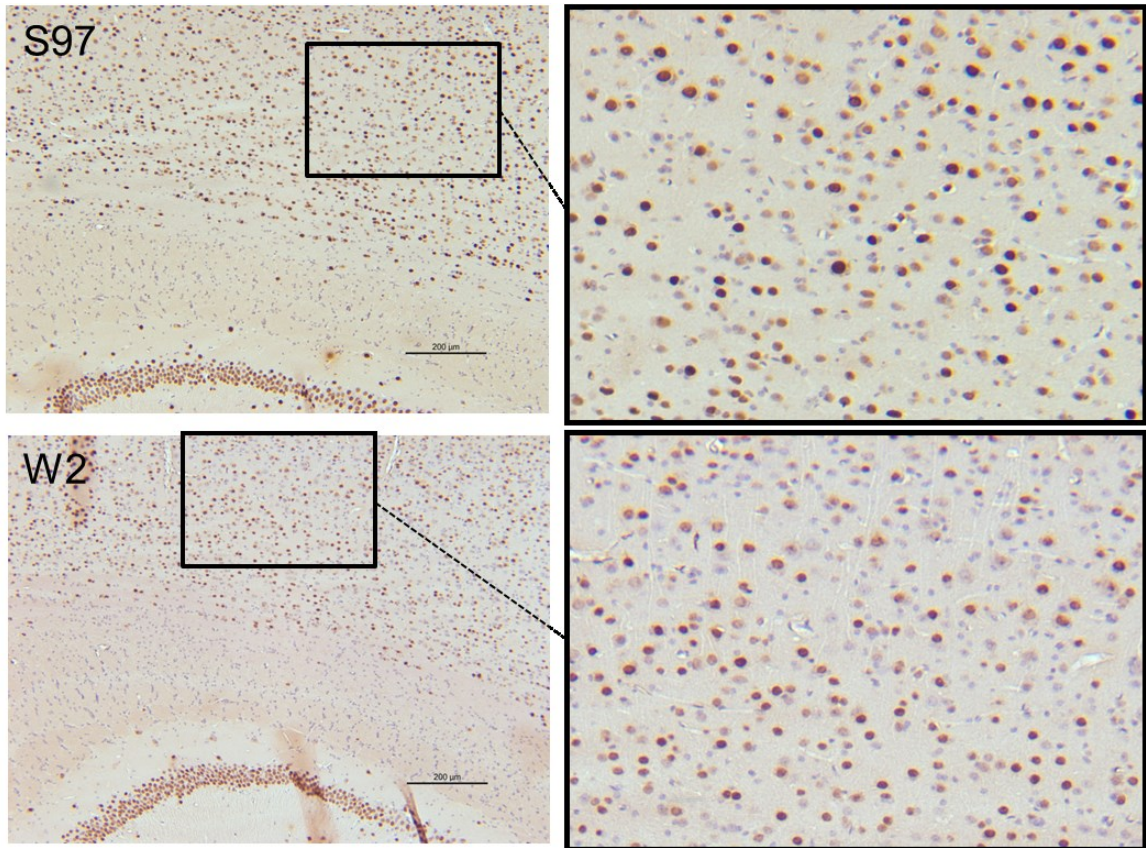


Figure 10: Forced gait stride lengths normalized to body lengths for S97 transgenic, W2 transgenic, and Nontransgenic (NT) males at 2 and 12 months-old. S97 transgenic and W2 transgenic mice have significantly shorter normalized stride length in all limbs (front right, front left, rear right, and rear left) as early as 2 months of age. NT 2mo, n=6, S97 transgenic 2mo, n=6, W2 transgenic 2mo, n=4, NT 12mo, n=5, S97 transgenic 12mo, n=4, W2 transgenic 12mo, n=4. Error bars represent standard deviations.



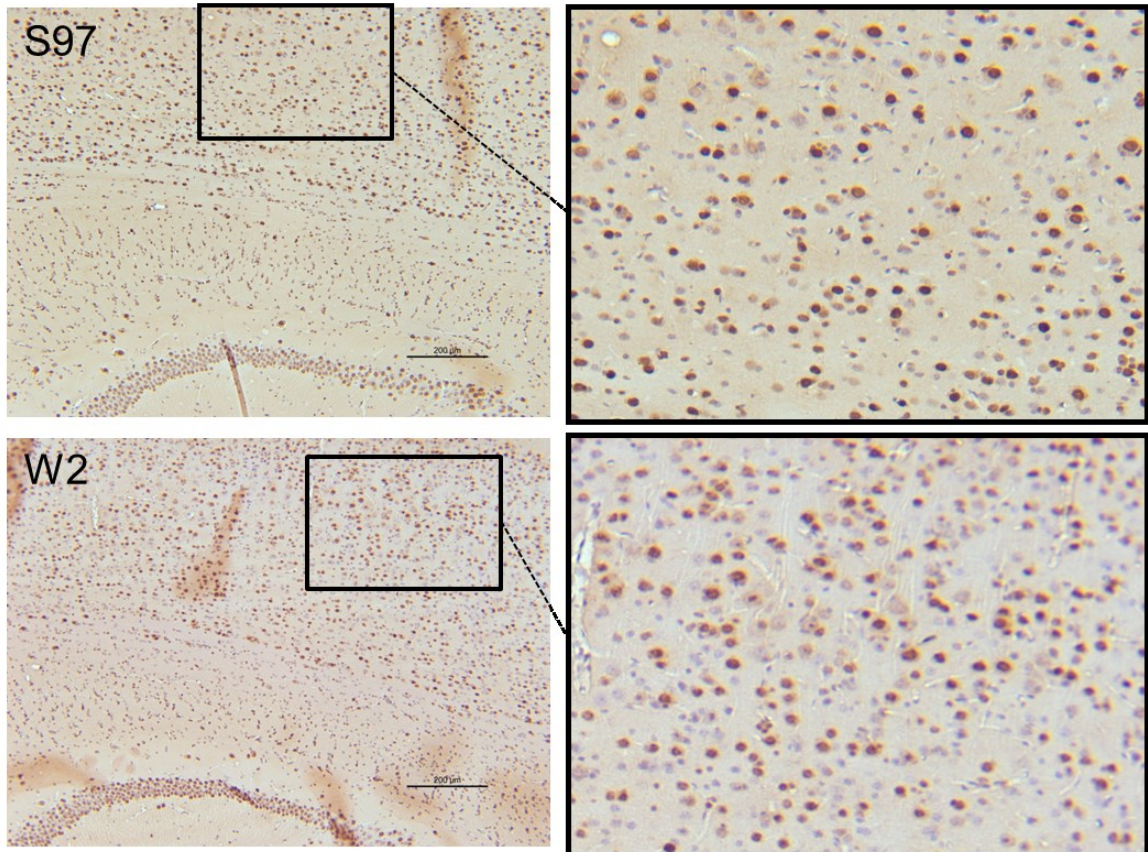
P value (Log-rank)
NT vs S97: 0.0035
NT vs W2: 0.0005
S97 vs W2: 0.1260

Figure 11: Kaplan-Meier survival curve for Nontransgenic (NT), S97 transgenic, and W2 transgenic male mice from the F3 generation. S97 transgenic and W2 transgenic mice have significantly shorter lifespans than NT mice. The difference in lifespan between S97 transgenic and W2 transgenic mice is not significant. NT, n=11, S97 transgenic, n=12, W2 transgenic, n=8. Four of twelve S97 transgenic mice were paralyzed at death, with onset of paralysis accompanied by a >10% weight loss at 26, 26, 27, and 28 months. Four of the eight W2 transgenic mice were paralyzed at death, with onset of paralysis accompanied by a >10% weight loss at 18, 21, 22, and 25 months.



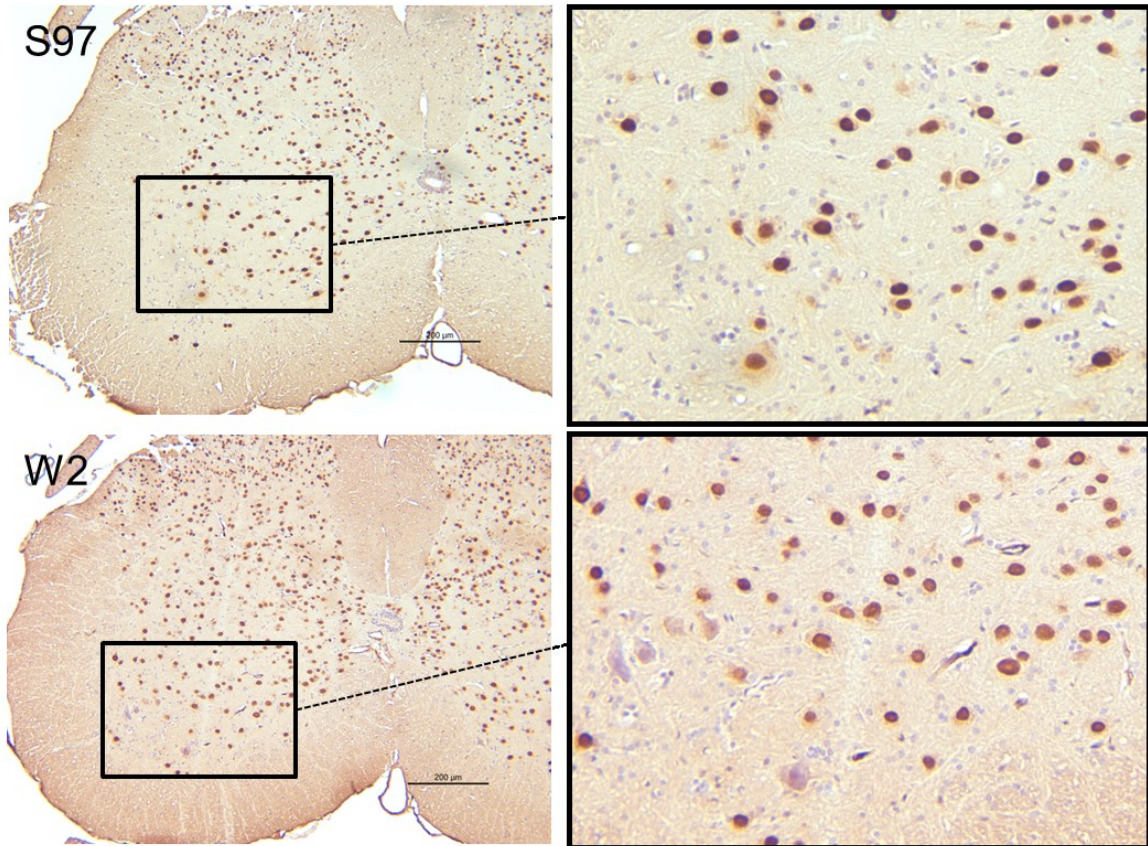
12mo, Novus mouse anti-human TDP-43

Figure 12: Immunohistochemical staining of cortical sections of S97 transgenic and W2 transgenic 12 month-old male mice with a mouse antibody specific for human TDP-43 (Novus, dark brown stain). Human TDP-43 is confined to the nucleus of neurons. No cytoplasmic inclusions are observed. Blue hemalum counterstain.



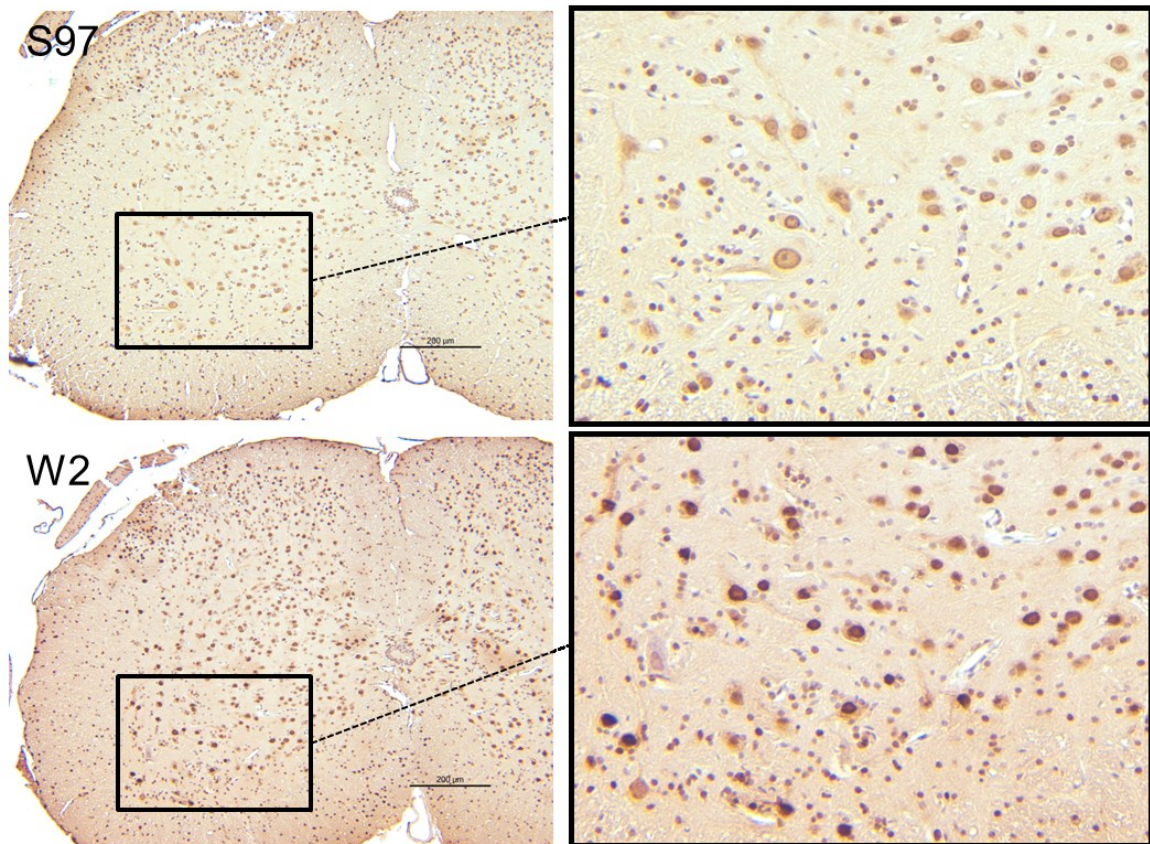
12mo, rabbit anti-TDP-43 (mouse + human)

Figure 13: Immunohistochemical staining of cortical sections of S97 transgenic and W2 transgenic 12 month-old male mice with a rabbit antibody detecting both mouse and human TDP-43 (Novus, dark brown stain). TDP-43 is confined to the nucleus of neurons and glia. No cytoplasmic inclusions are observed. Blue hemalum counterstain.



12mo, Novus mouse anti-human TDP-43

Figure 14: Immunohistochemical staining of lumbar spinal cord sections of S97 transgenic and W2 transgenic 12 month-old male mice with a mouse antibody specific for human TDP-43 (Novus, dark brown stain). Human TDP-43 is confined to the nucleus of neurons. No cytoplasmic inclusions are observed. Blue hemalum counterstain.



12mo, rabbit anti-TDP-43 (mouse + human)

Figure 15: Immunohistochemical staining of lumbar spinal cord sections of S97 transgenic and W2 transgenic 12 month-old male mice with a rabbit antibody detecting both mouse and human TDP-43 (Novus, dark brown stain). TDP-43 is confined to the nucleus of neurons and glia. No cytoplasmic inclusions are observed. Blue hemalum counterstain. Difference in staining intensity likely due to different diaminobenzidine developing times.

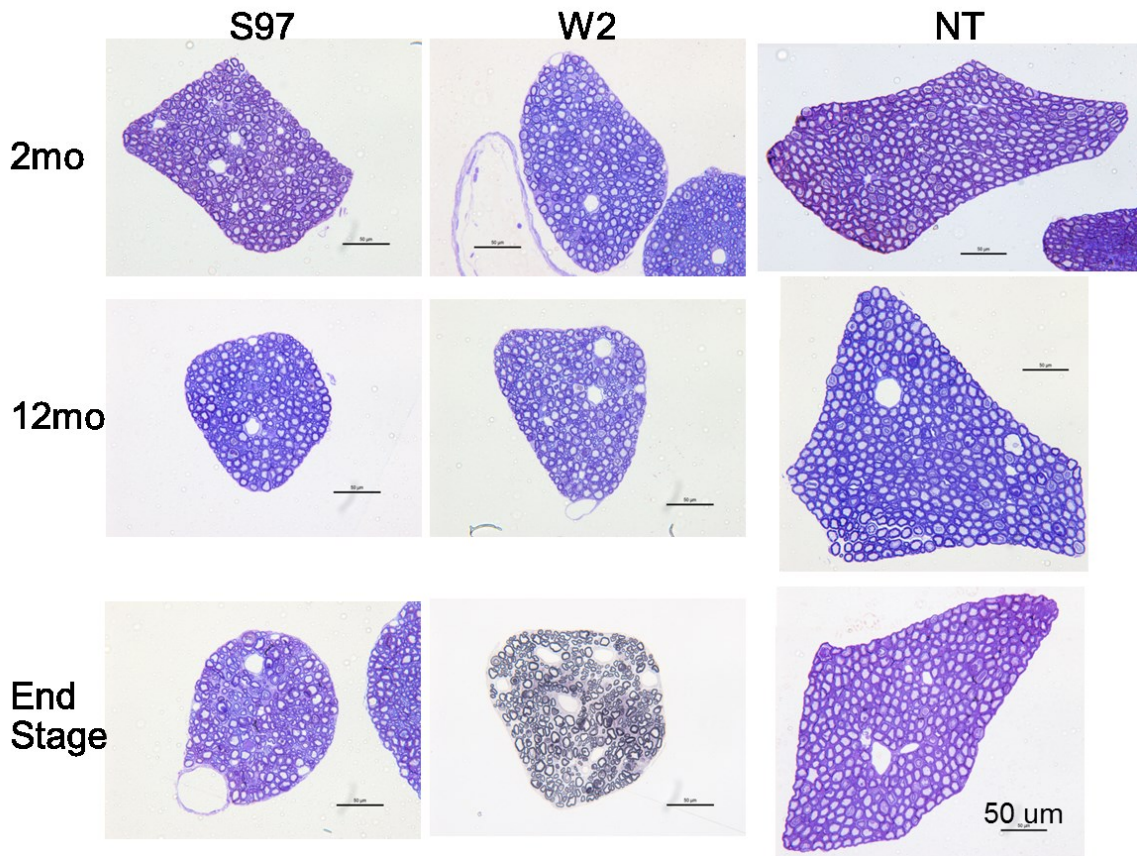


Figure 16: Electron microscopy thick sections of L3 ventral roots from S97 transgenic, W2 transgenic, and Nontransgenic (NT) 2 and 12-month old and end-stage male mice. Roots from S97 transgenic and W2 transgenic mice are noticeably smaller than roots from NT mice at all ages.

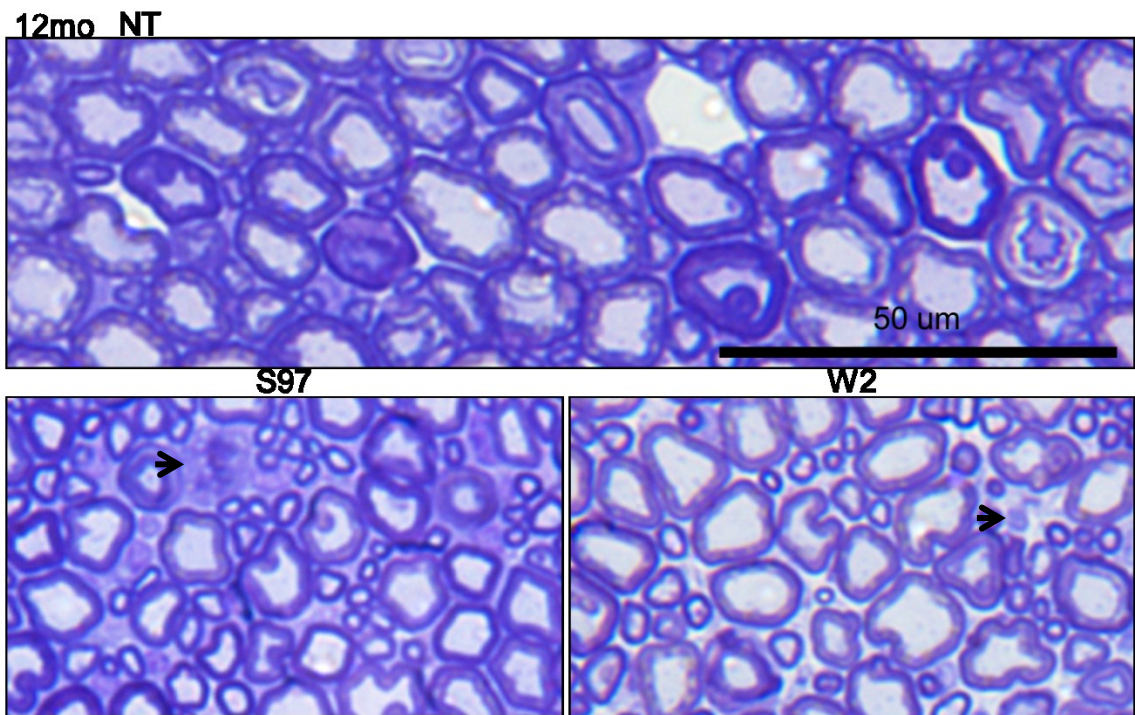


Figure 17: Closer view of electron microscopy thick sections of L3 ventral roots from S97 transgenic, W2 transgenic, and Nontransgenic (NT) 12-month-old male mice. Roots from S97 transgenic and W2 transgenic mice show a reduced number of large myelinated axons, increasing the visibility of smaller axons. Roots from transgenic mice also show the presence of large vacuoles.

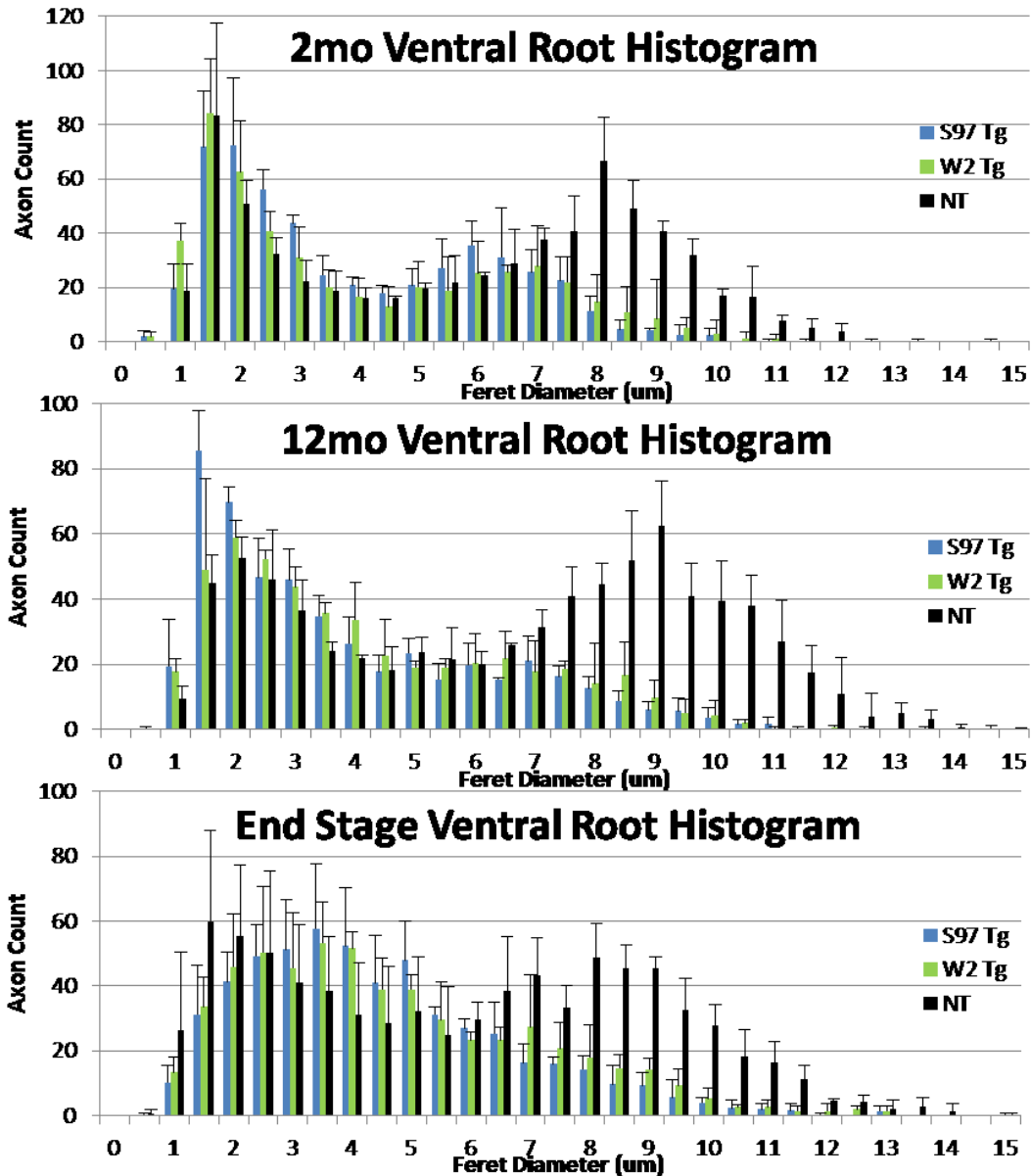


Figure 18: Histograms displaying the distribution of axon diameters in L3 ventral roots from S97 transgenic, W2 transgenic, and Nontransgenic (NT) 2- and 12-month-old and end-stage male mice. NT mice show a bimodal distribution of axon diameters at all ages. Meanwhile, S97 transgenic and W2 transgenic animals have lost a portion of the large-diameter (Feret diameter $\geq 4.5\mu\text{m}$) axons before the age of 2 months. For each genotype and age group, $n=3$. Error bars represent standard deviations.

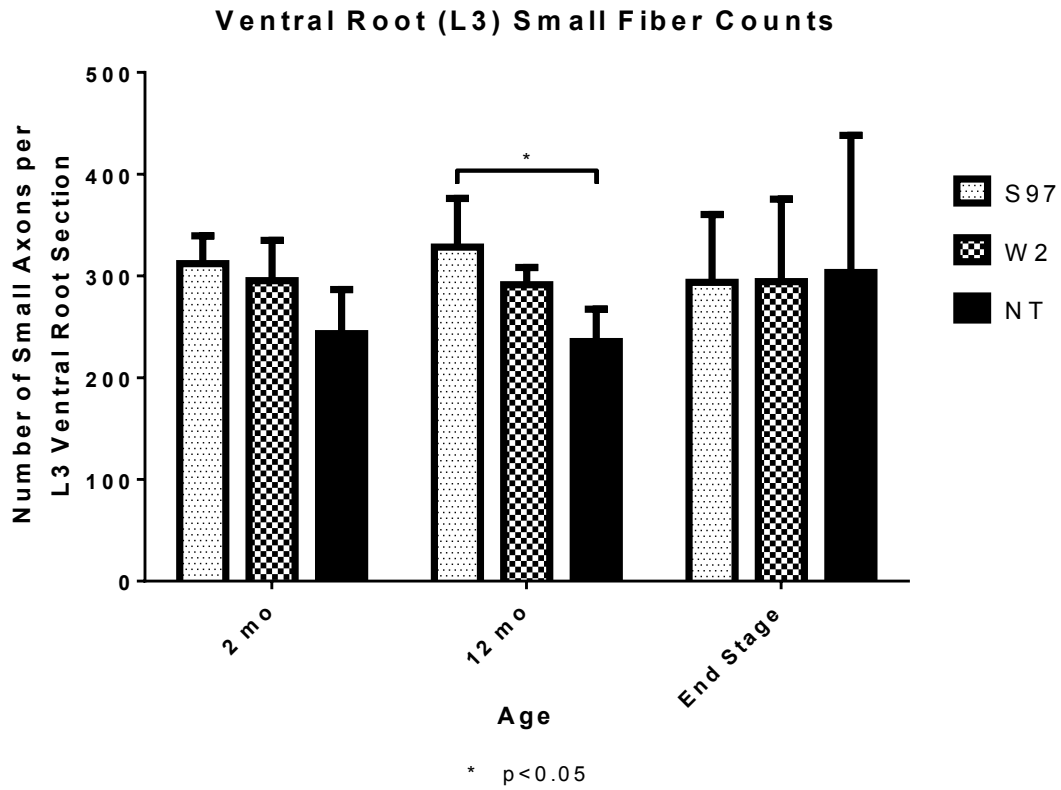


Figure 19: Quantification of the number of small axons (Feret diameter < 4.5) in L3 ventral roots from S97 transgenic, W2 transgenic, and Nontransgenic (NT) 2- and 12-month-old and end-stage male mice. The number of small axons remains consistent as animals age. The numbers of small axons in S97 transgenic and W2 transgenic ventral roots are slightly increased compared to the number of small axons in NT roots. This difference is significant when comparing S97 transgenic 12-month-old roots and NT 12-month-old roots. Error bars represent standard deviations.

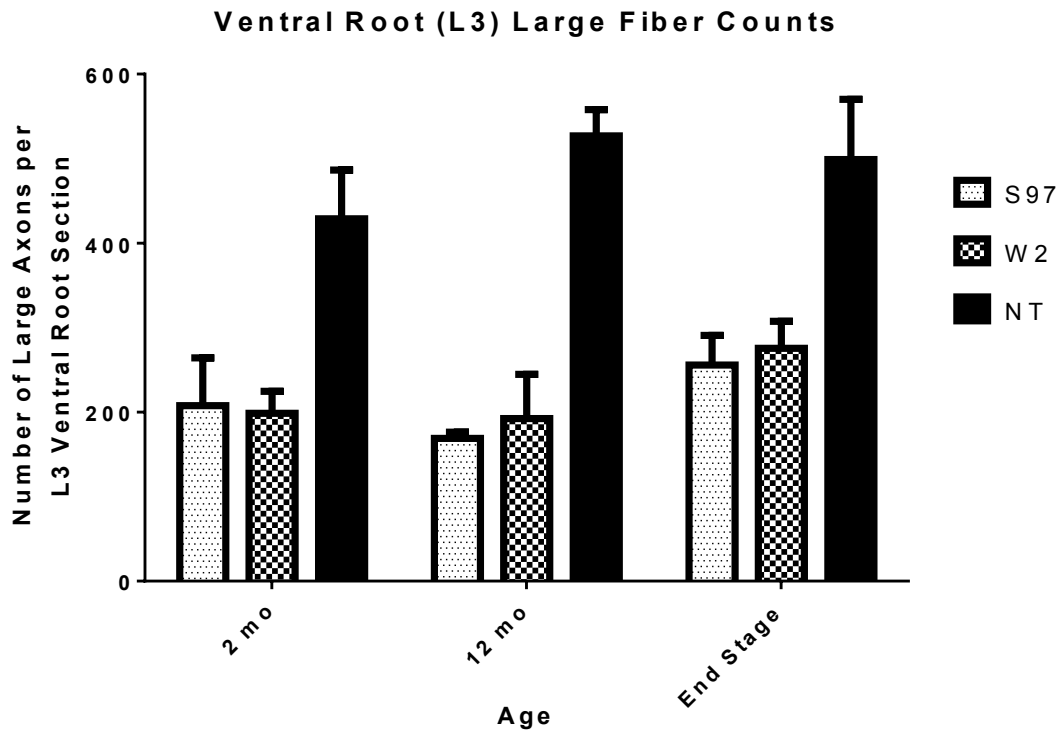


Figure 20: Quantification of the number of large axons (Feret diameter $\geq 4.5\mu\text{m}$) in L3 ventral roots from S97 transgenic, W2 transgenic, and Nontransgenic (NT) 2- and 12-month-old and end-stage male mice. At each age, the numbers of large axons in S97 transgenic and W2 transgenic ventral roots are significantly decreased compared to the number of large axons in NT roots. Error bars represent standard deviations.

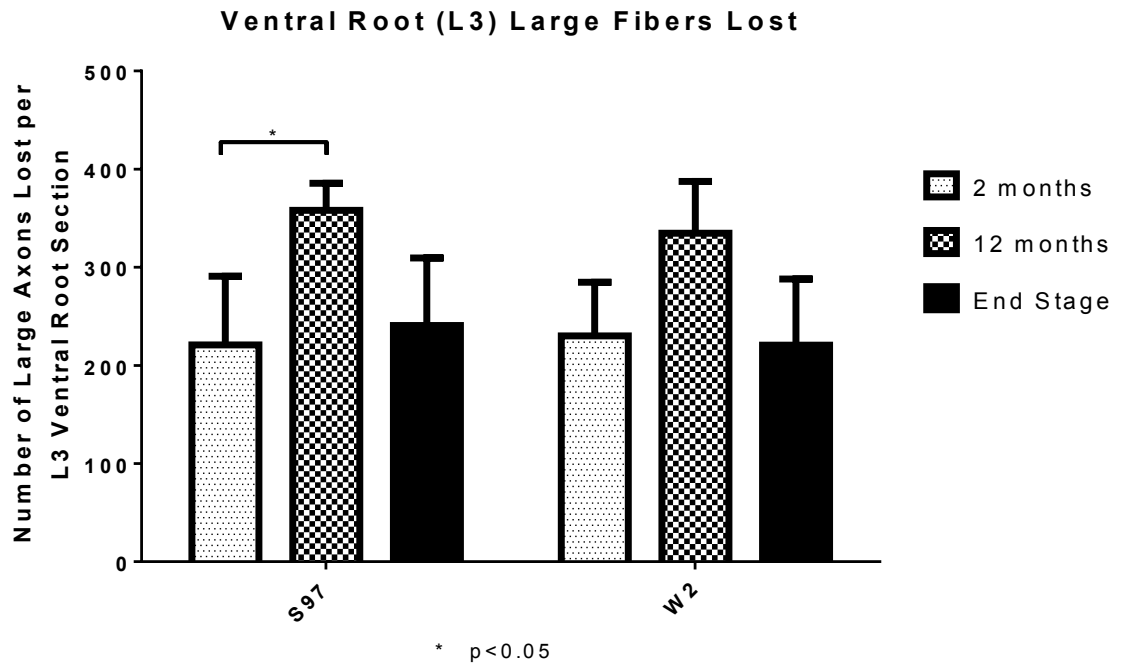


Figure 21: Quantification of the number of large axons (Feret diameter $\geq 4.5\mu\text{m}$) lost in L3 ventral roots from S97 and W2 2- and 12-month-old and end-stage transgenic male mice, compared to L3 roots from NT animals at each age. Two-month-old S97 and W2 transgenic mice have already lost a large number of large axons. However, the number of large axons lost peaks at the age of 12 months. Error bars represent standard deviations.

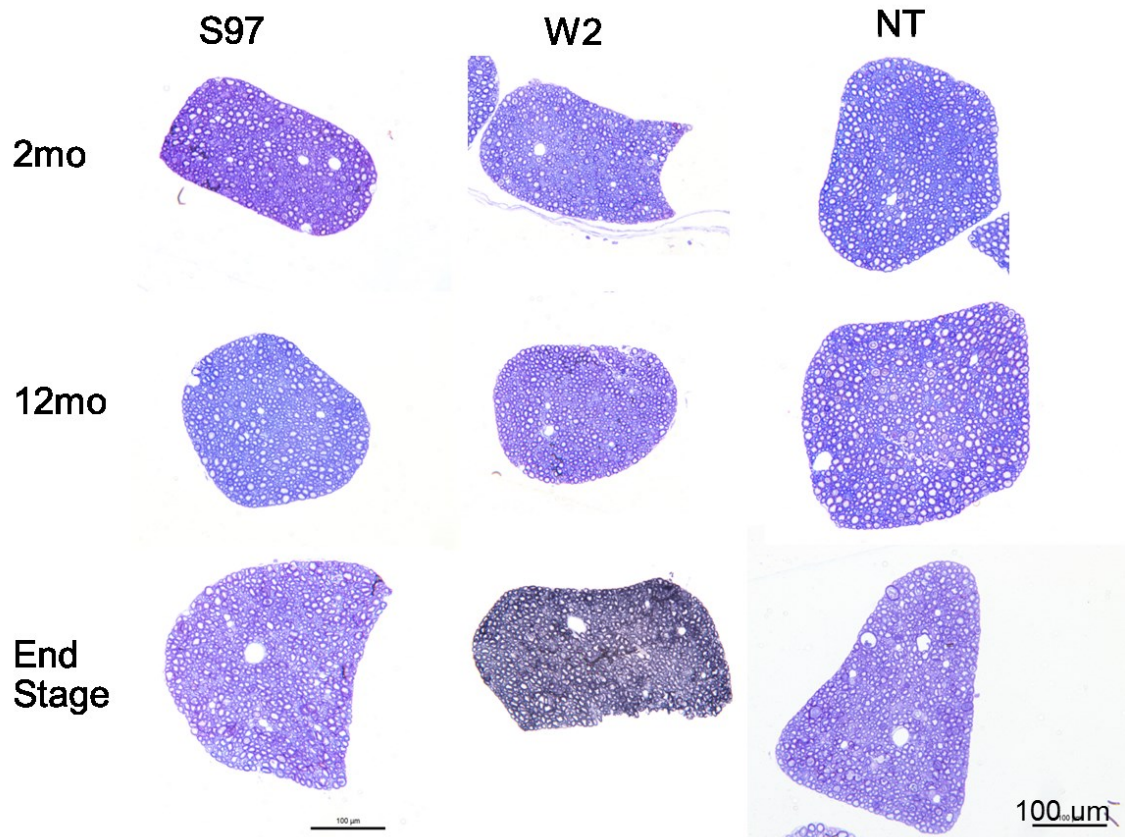


Figure 22: Electron microscopy thick sections of L3 dorsal roots from S97 transgenic, W2 transgenic, and Nontransgenic (NT) 2 and 12-month old and end-stage male mice. Roots from S97 and W2 transgenic mice are noticeably smaller than roots from NT mice at all ages.

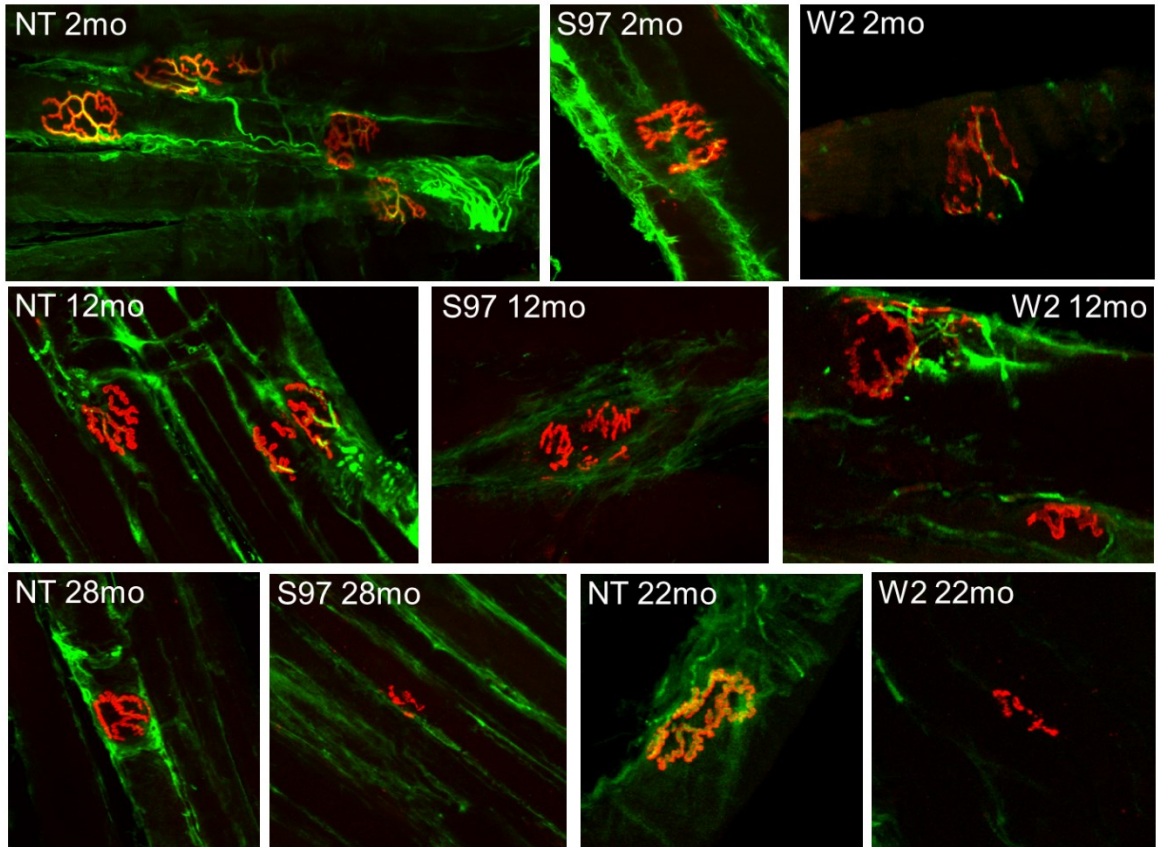


Figure 23: Staining for neuromuscular junctions in thick sections of gastrocnemius muscles from S97 transgenic, W2 transgenic, and Nontransgenic (NT) 2- and 12-month-old and end-stage male mice. SMI-312 neurofilament and synaptophysin staining in green and α -bungarotoxin staining in red, with overlap indicating an innervated neuromuscular junction.

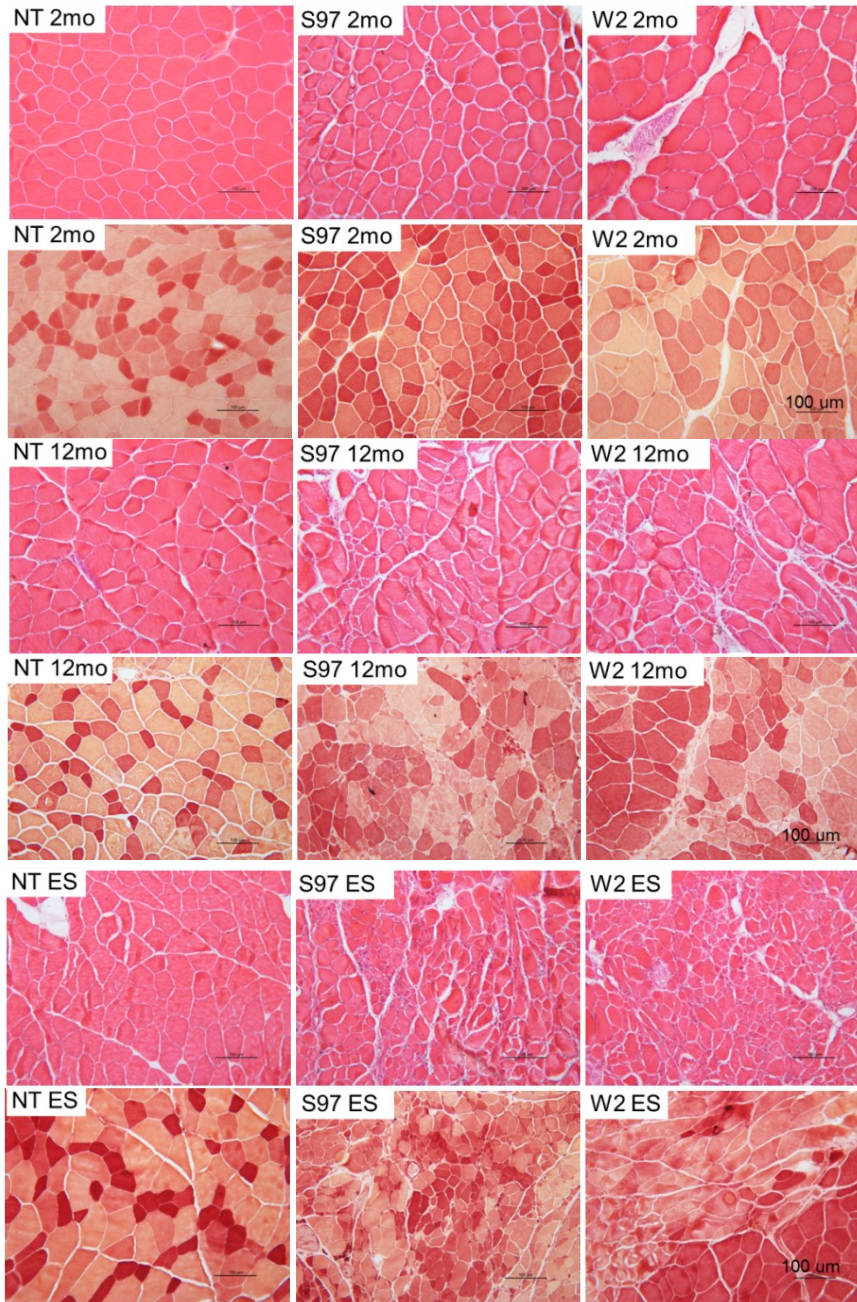


Figure 24: Hematoxylin and eosin staining and esterase staining of quadriceps muscles from S97 transgenic, W2 transgenic, and Nontransgenic (NT) 2- and 12-month-old and end-stage male mice. H+E staining shows progressively increasing disorganization and angulated fibers in S97 and W2 muscle as the animals age. Esterase staining showing evidence of fiber-type grouping in the S97 and W2 aged transgenic mouse muscle.

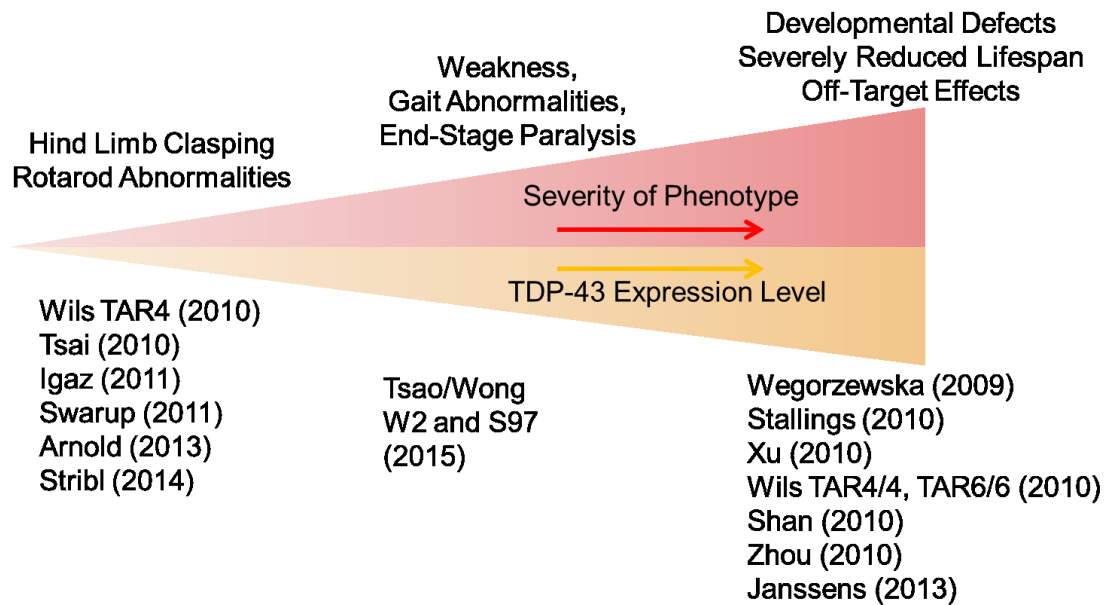


Figure 25: Schematic framework for published TDP-43 transgenic mouse models. Many of the early models had very high TDP-43 levels and severe developmental or early life defects, prompting a response to develop models with lower TDP-43 levels. However, these mice uniformly did not reach end-stage paralysis. The W2 and S97 mouse lines live well into adult age but develop weakness, gait abnormalities, and paralysis at end-stage near 2 years of age.

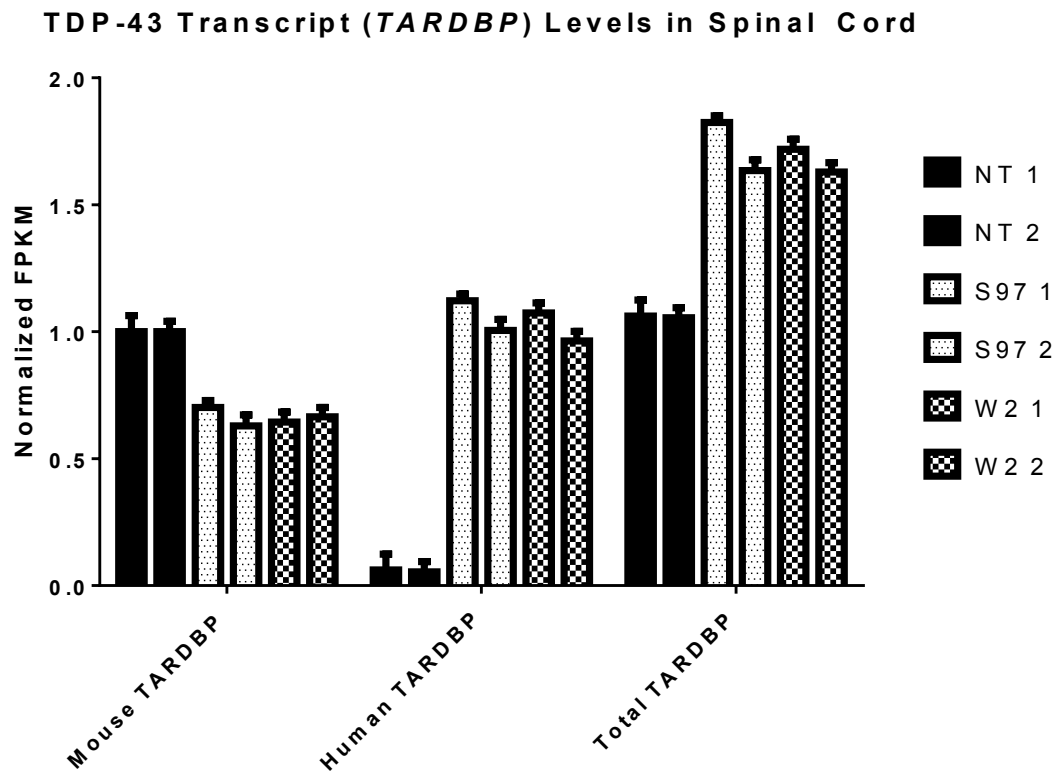


Figure 26: *TARDBP* expression levels normalized to the mouse *TARDBP* expression level in Nontransgenic (NT) mice. Data from Cufflinks processing of RNA Sequencing data from 6-week-old male S97 transgenic, W2 transgenic, and NT spinal cords. In mice expressing transgenic hTDP-43, the mouse *TARDBP* expression is diminished. Error bars represent standard deviations.

Differences in Transcript Level

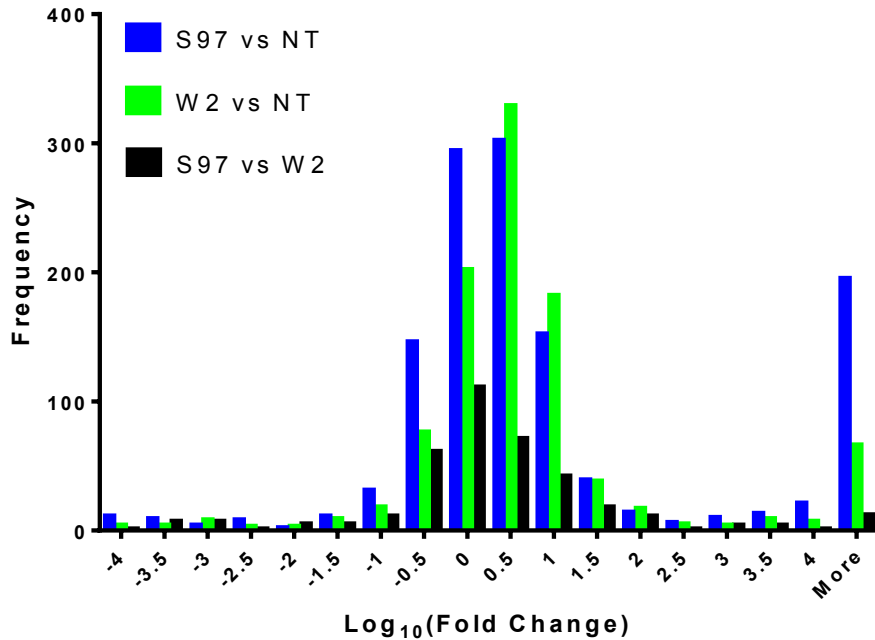


Figure 27: Histogram showing the number and significance of transcript level differences when comparing S97 transgenics to Nontransgenic (NT) mice, when comparing W2 transgenics to NT mice, and when comparing S97 transgenics to W2 transgenics. Data from Cufflinks processing of RNA Sequencing data from 6-week-old male S97 transgenic, W2 transgenic, and NT spinal cords. The transgenic S97 and W2 transcriptomes are relatively similar, while each transgenic transcriptome is different from the NT transcriptome.

Ref_ID Specific Transcript	Gene	FPKM (S97 NT)	FPKM (W2 NT)	FPKM (S97 Tg 1)	FPKM (S97 Tg 2)	FPKM (W2 Tg 1)	FPKM (W2 Tg 2)
uc007jkv.1	<i>Arhgap44</i>	5.92835	12.0668	35.0676	33.132	40.8015	42.8396
uc008cxj.1	<i>Trem2</i>	6.59473	5.53411	11.7785	17.2804	29.465	18.1659
uc007qmf.2	<i>S1pr3</i>	1.82184	2.02649	4.48358	6.96912	6.57204	6.06923
uc008wve.1	<i>Hadhb</i>	1.08464	1.13788	4.08408	2.99469	2.63488	3.65313
uc008pir.2	<i>P2ry12</i>	1.42224	2.07875	3.49218	5.26531	5.77299	4.06511
uc008ofd.1	<i>Ctsz</i>	32.0753	26.5907	53.5797	65.4923	90.7756	77.2377
uc007zbv.1	<i>Dtx3l</i>	1.08282	1.00418	2.04473	2.31244	2.70127	2.82641
uc009dlm.1	<i>Ret</i>	1.83405	1.42241	4.05329	3.7845	3.87296	2.85755

Figure 28: Selection of transcripts with higher expression levels in S97 and W2 transgenic mice compared to Nontransgenic (NT) mice. Data from Cufflinks processing of RNA Sequencing data from 6-week-old male S97 transgenic, W2 transgenic, and NT spinal cords. uc007jkv.1 is *ARHGAP44* Transcript Variant 1.

Ref_ID Specific Transcript	Gene	FPKM (S97 NT)	FPKM (W2 NT)	FPKM (S97 Tg 1)	FPKM (S97 Tg 2)	FPKM (W2 Tg 1)	FPKM (W2 Tg 2)
uc007cdf.2	<i>Kif1a</i>	8.8418	8.77671	4.77749	4.50546	4.29287	4.08203
uc008onm.1	<i>Opr11</i>	7.23299	6.22733	5.95137	3.39032	4.01406	2.01595
uc009gyc.1	<i>Kcnj11</i>	13.9285	11.1561	8.7796	7.46934	4.8396	5.01667
uc008ggw.1	<i>Tm7sf2</i>	19.9626	23.2435	10.6269	11.4435	12.3079	9.88884
uc008vvg.1	<i>Tardbp</i>	11.4023	11.4098	8.00262	7.1736	7.34353	7.57883

Figure 29: Selection of transcripts with lower expression levels in S97 and W2 transgenic mice compared to Nontransgenic (NT) mice. Data from Cufflinks processing of RNA Sequencing data from 6-week-old male S97 transgenic, W2 transgenic, and NT spinal cords.

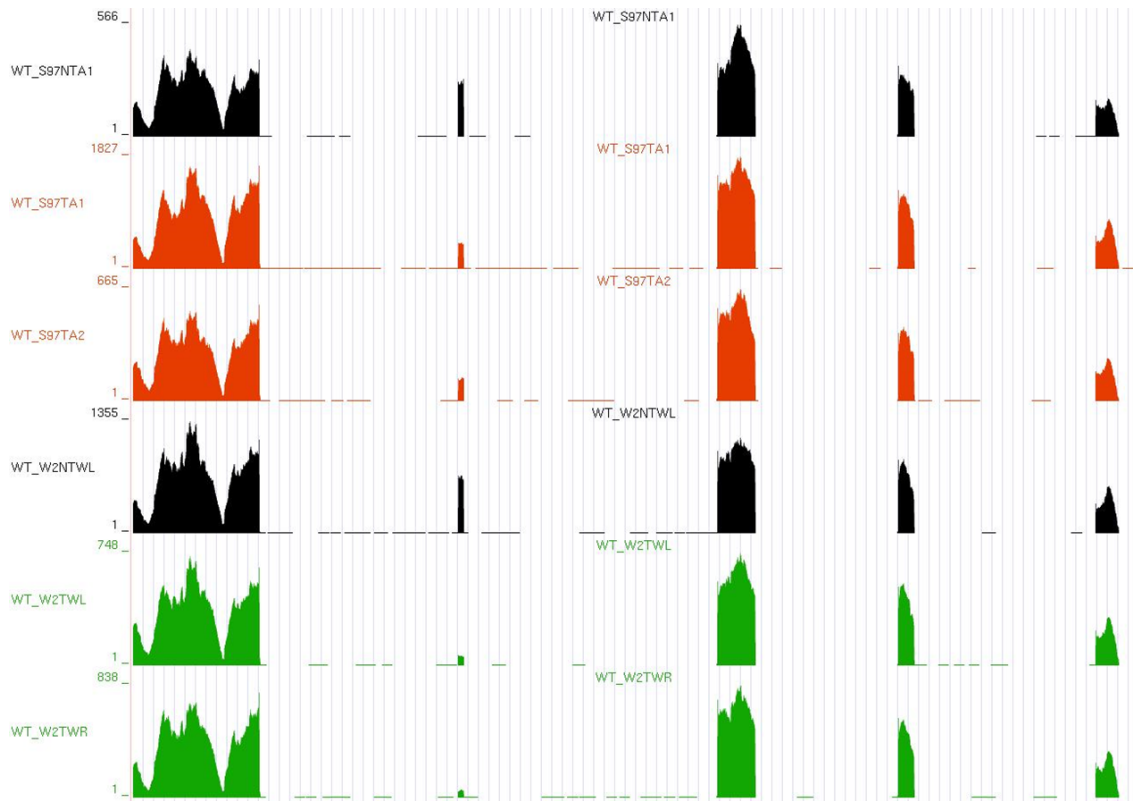


Figure 30: *ARHGAP44* expression in 6-week-old male S97 transgenic (WT_S97TA1 and WT_S97TA2), W2 transgenic (WT_W2TWL and WT_W2TWR), and Nontransgenic (NT) (WT_S97NTA1 and WT_W2NTWL) spinal cords, mapped using the UCSC Genome Browser using Tophat-processed RNA Sequencing data. In the transgenic animals, one exon has been spliced out.

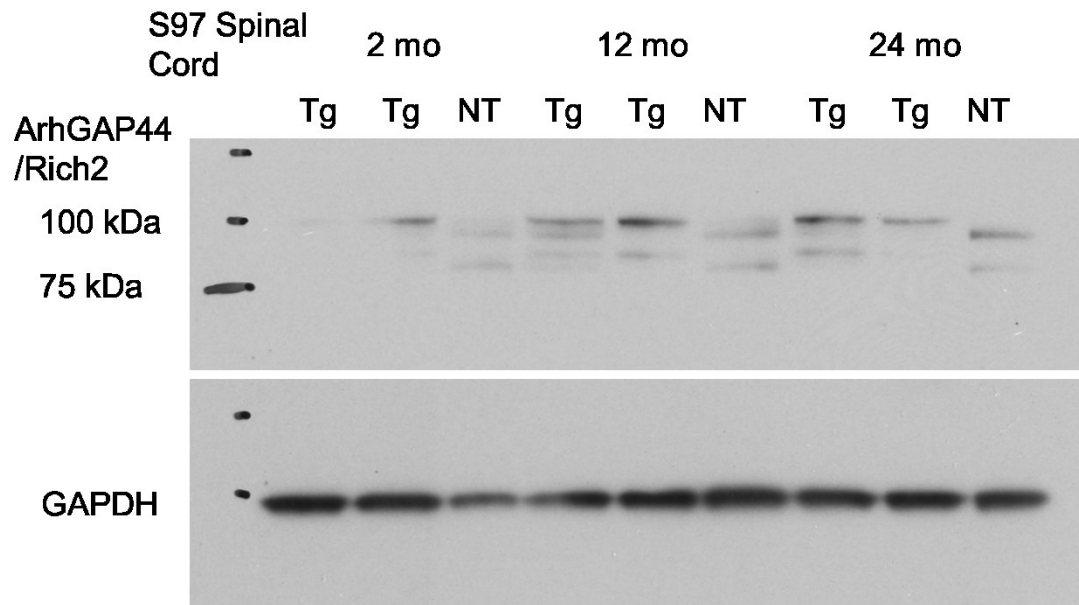
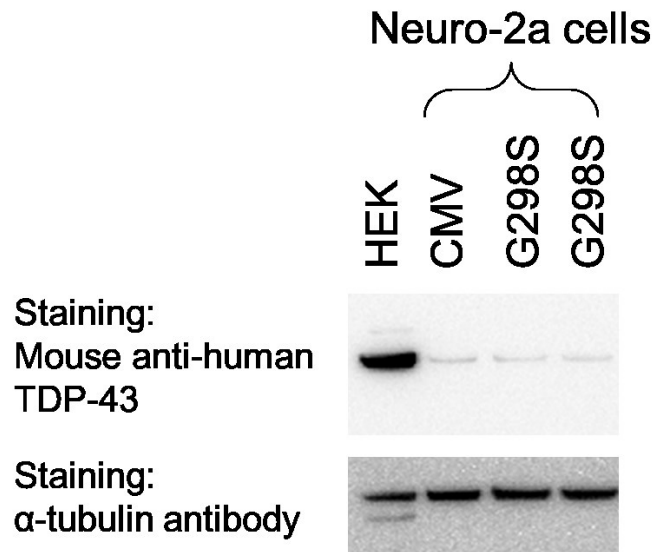


Figure 31: Western blot showing ArhGAP44/Rich2 expression in 2-, 12-, and 24-month-old male S97 transgenic and Nontransgenic (NT) spinal cord samples. At all ages, the major band (~100 kDa) in transgenic animals appears to be larger than the major band in NT animals. GAPDH acts as a loading control.

SUPPLEMENTAL FIGURES



Supplemental Figure 1: Testing for expression of human TDP-43 in Neuro-2a mouse neuroblastoma cells transfected with pTSC-TDP-G298S. “HEK” is lysate from untransfected HEK-293 cells, used as a positive control for human TDP-43 staining. “CMV”, another positive control, is lysate from N2a cells transfected with a plasmid expressing hTDP-43 under a CMV promoter. Staining with α -tubulin antibody is used to show equal loading.

Homo sapiens TAR DNA binding protein (TARDBP), mRNA
 Sequence ID: [ref|NM_007375.3|](#) Length: 4236 Number of Matches: 1

Score	Expect	Identities	Gaps	Strand
819 bits(443)	0.0	443/443(100%)	0/443(0%)	Plus/Plus
CDS: Putative 1	1	I A Q S L C G E D L I I K G I S V H I S		
Query	1	ATTGGCGAGTCTCTTTGTGGAGAGGACTTGATCATTAAGGAATCAGCGTTCATATATCC	60	
Sbjct	849	908	
CDS: TAR DNA-binding	239	I A Q S L C G E D L I I K G I S V H I S		
CDS: Putative 1	21	N A E P K H N S N R Q L E R S G R F G G		
Query	61	AATGCCGAACCTAAGCACAATAGCAATAGACAGTTAGAAAGAAAGTGAAGATTGGTGGT	120	
Sbjct	909	968	
CDS: TAR DNA-binding	259	N A E P K H N S N R Q L E R S G R F G G		
CDS: Putative 1	41	N P G G F G N Q G G F G N S R G G G A G		
Query	121	AATCCAGGTGGCTTTGGGAATCAGGTTGGATTGGTAAAGCAGAGGGGGTGGAGCTGCT	180	
Sbjct	969	1028	
CDS: TAR DNA-binding	279	N P G G F G N Q G G F G N S R G G G A G		
CDS: Putative 1	61	L G N N Q G S N M G G G M N F G A F S I		
Query	181	TTGGGAACAATCAAGGTAGTAATATGGGTGGTGGGATGAACCTTTGGTCCGTTCAAGCATT	240	
Sbjct	1029	1088	
CDS: TAR DNA-binding	299	L G N N Q G S N M G G G M N F G A F S I		
CDS: Putative 1	81	N P A M M A A A Q A A L Q S S W G M M G		
Query	241	AATCCAGCCATGATGGCTGCCGCCAGGACAGCACTACAGAGCAGTTGGGGTATGATGGCC	300	
Sbjct	1089	1148	
CDS: TAR DNA-binding	319	N P A M M A A A Q A A L Q S S W G M M G		
CDS: Putative 1	101	M L A S Q Q N Q S G P S G N N Q N Q G N		
Query	301	ATGTTAGCCAGCCAGCAGAACCCAGTCAGGCCATCGGGTAATAACCAAACCAAGGCAAC	360	
Sbjct	1149	1208	
CDS: TAR DNA-binding	339	M L A S Q Q N Q S G P S G N N Q N Q G N		
CDS: Putative 1	121	M Q R E P N Q A F G S G N N S Y S G S N		
Query	361	ATGCAGAGGGAGCCAAACAGGCCTTCGGTTCCTGGAATAACTCTTATAGTGGCTCTAAT	420	
Sbjct	1209	1268	
CDS: TAR DNA-binding	359	M Q R E P N Q A F G S G N N S Y S G S N		
CDS: Putative 1	141	S G A A I G W G		
Query	421	TCTGGTGCAGCAATTGGTTGGG 443		
Sbjct	1269 1291		
CDS: TAR DNA-binding	379	S G A A I G W G		

W2 Exon 6

Homo sapiens TAR DNA binding protein (TARDBP), mRNA
 Sequence ID: [ref|NM_007375.3|](#) Length: 4236 Number of Matches: 1

Score	Expect	Identities	Gaps	Strand
813 bits(440)	0.0	442/443(99%)	0/443(0%)	Plus/Plus
CDS: Putative 1	1	I A Q S L C G E D L I I K G I S V H I S		
Query	1	ATTGGCGAGTCTCTTTGTGGAGAGGACTTGATCATTAAGGAATCAGCGTTCATATATCC	60	
Sbjct	849	908	
CDS: TAR DNA-binding	239	I A Q S L C G E D L I I K G I S V H I S		
CDS: Putative 1	21	N A E P K H N S N R Q L E R S G R F G G		
Query	61	AATGCCGAACCTAAGCACAATAGCAATAGACAGTTAGAAAGAAAGTGAAGATTGGTGGT	120	
Sbjct	909	968	
CDS: TAR DNA-binding	259	N A E P K H N S N R Q L E R S G R F G G		
CDS: Putative 1	41	N P G G F G N Q G G F G N S R G G G A S		
Query	121	AATCCAGGTGGCTTTGGGAATCAGGTTGGATTGGTAAAGCAGAGGGGGTGGAGCTGCT	180	
Sbjct	969G..	1028	
CDS: TAR DNA-binding	279	N P G G F G N Q G G F G N S R G G G A G		
CDS: Putative 1	61	L G N N Q G S N M G G G M N F G A F S I		
Query	181	TTGGGAACAATCAAGGTAGTAATATGGGTGGTGGGATGAACCTTTGGTCCGTTCAAGCATT	240	
Sbjct	1029	1088	
CDS: TAR DNA-binding	299	L G N N Q G S N M G G G M N F G A F S I		
CDS: Putative 1	81	N P A M M A A A Q A A L Q S S W G M M G		
Query	241	AATCCAGCCATGATGGCTGCCGCCAGGACAGCACTACAGAGCAGTTGGGGTATGATGGCC	300	
Sbjct	1089	1148	
CDS: TAR DNA-binding	319	N P A M M A A A Q A A L Q S S W G M M G		
CDS: Putative 1	101	M L A S Q Q N Q S G P S G N N Q N Q G N		
Query	301	ATGTTAGCCAGCCAGCAGAACCCAGTCAGGCCATCGGGTAATAACCAAACCAAGGCAAC	360	
Sbjct	1149	1208	
CDS: TAR DNA-binding	339	M L A S Q Q N Q S G P S G N N Q N Q G N		
CDS: Putative 1	121	M Q R E P N Q A F G S G N N S Y S G S N		
Query	361	ATGCAGAGGGAGCCAAACAGGCCTTCGGTTCCTGGAATAACTCTTATAGTGGCTCTAAT	420	
Sbjct	1209	1268	
CDS: TAR DNA-binding	359	M Q R E P N Q A F G S G N N S Y S G S N		
CDS: Putative 1	141	S G A A I G W G		
Query	421	TCTGGTGCAGCAATTGGTTGGG 443		
Sbjct	1269 1291		
CDS: TAR DNA-binding	379	S G A A I G W G		

S97 Exon 6

Supplemental Figure 2: Sequencing of human *TARDBP* from DNA isolated from W2 or S97 mice. S97 DNA shows the single G to A substitution, resulting in the glycine to serine substitution in the human TDP-43 protein.

Supplemental Figure 3: Antibody Table

Antigen	Antigen Type	Antibody Species	Manufacturer
Human TDP-43 (2E2-D3) (Zhang et al, 2008)	DNA/RNA Binding Protein	Mouse	Novus
Mouse TDP-43 (N-Term) 10782-2	DNA/RNA Binding Protein	Rabbit	Proteintech
Mouse TDP-43 (C-Term) 12892-1	DNA/RNA Binding Protein	Rabbit	Proteintech
Phospho 409/410 TDP-43	DNA/RNA Binding Protein	Rabbit	Cosmo Bio
Synaptophysin (Z66)	Synaptic Vesicle	Rabbit	Life Technologies
ChAT (AB144P)	Motor Neurons	Goat	Millipore
GAPDH (GAPDH-71.1)	Metabolism	Mouse	Sigma
Ubiquitin	Signaling tag	Rabbit	Dako
SMI-31	Neurofilament NF-H	Mouse	Covance
SMI-32	Neurofilament NF-H	Mouse	Covance
SMI-312 (SMI-312R)	Neurofilament	Mouse	Covance
GFAP	Astrocytic marker	Rabbit	Dako
ArhGAP44 / RICH2 (ab93627)	RhoGAP	Rabbit	Abcam

REFERENCES

Arai T, Hasegawa M, Akiyama H, et al. TDP-43 is a component of ubiquitin-positive tau-negative inclusions in frontotemporal lobar degeneration and amyotrophic lateral sclerosis. *Biochem Biophys Res Commun.* 2006;351(3):602-11.

Arnold ES, Ling SC, Huelga SC, et al. ALS-linked TDP-43 mutations produce aberrant RNA splicing and adult-onset motor neuron disease without aggregation or loss of nuclear TDP-43. *Proc Natl Acad Sci USA.* 2013;110(8):E736-45.

Ayala YM, Pantano S, D'ambrogio A, et al. Human, *Drosophila*, and *C.elegans* TDP43: nucleic acid binding properties and splicing regulatory function. *J Mol Biol.* 2005;348(3):575-88.

Ayala YM, Zago P, D'ambrogio A, et al. Structural determinants of the cellular localization and shuttling of TDP-43. *J Cell Sci.* 2008;121(Pt 22):3778-85.

Ayala YM, De conti L, Avendaño-vázquez SE, et al. TDP-43 regulates its mRNA levels through a negative feedback loop. *EMBO J.* 2011;30(2):277-88.

Barmada SJ, Skibinski G, Korb E, Rao EJ, Wu JY, Finkbeiner S. Cytoplasmic mislocalization of TDP-43 is toxic to neurons and enhanced by a mutation associated with familial amyotrophic lateral sclerosis. *J Neurosci.* 2010;30(2):639-49.

Beare JE, Morehouse JR, Devries WH, et al. Gait analysis in normal and spinal contused mice using the TreadScan system. *J Neurotrauma*. 2009;26(11):2045-56.

Benajiba L, Le Ber I, Camuzat A, et al. TARDBP mutations in motoneuron disease with frontotemporal lobar degeneration. *Ann Neurol*. 2009;65(4):470-3.

Bennion Callister J, Pickering-Brown SM. Pathogenesis/genetics of frontotemporal dementia and how it relates to ALS. *Exp Neurol*. 2014;262 Pt B:84-90.

Blankenberg D, Gordon A, Von kuster G, et al. Manipulation of FASTQ data with Galaxy. *Bioinformatics*. 2010;26(14):1783-5.

Borchelt DR, Davis J, Fischer M, et al. A vector for expressing foreign genes in the brains and hearts of transgenic mice. *Genet Anal*. 1996;13(6):159-63.

Borroni B, Archetti S, Del bo R, et al. TARDBP mutations in frontotemporal lobar degeneration: frequency, clinical features, and disease course. *Rejuvenation Res*. 2010;13(5):509-17.

Bose JK, Wang IF, Hung L, Tarn WY, Shen CK. TDP-43 overexpression enhances exon 7 inclusion during the survival of motor neuron pre-mRNA splicing. *J Biol Chem*. 2008;283(43):28852-9.

- Brujin LI, Becher MW, Lee MK, et al. ALS-linked SOD1 mutant G85R mediates damage to astrocytes and promotes rapidly progressive disease with SOD1-containing inclusions. *Neuron*. 1997;18(2):327-38.
- Brujin LI, Miller TM, Cleveland DW. Unraveling the mechanisms involved in motor neuron degeneration in ALS. *Annu Rev Neurosci*. 2004;27:723-49.
- Budini M, Romano V, Avendaño-vázquez SE, Bembich S, Buratti E, Baralle FE. Role of selected mutations in the Q/N rich region of TDP-43 in EGFP-12xQ/N-induced aggregate formation. *Brain Res*. 2012;1462:139-50.
- Buratti E, Baralle FE. Multiple roles of TDP-43 in gene expression, splicing regulation, and human disease. *Front Biosci*. 2008;13:867-78.
- Buratti E, Brindisi A, Pagani F, Baralle FE. Nuclear factor TDP-43 binds to the polymorphic TG repeats in CFTR intron 8 and causes skipping of exon 9: a functional link with disease penetrance. *Am J Hum Genet*. 2004;74(6):1322-5.
- Buratti E, Romano M, Baralle FE. TDP-43 high throughput screening analyses in neurodegeneration: advantages and pitfalls. *Mol Cell Neurosci*. 2013;56:465-74.
- Carlson BM, Borisov AB, Dedkov EI, et al. Effects of long-term denervation on skeletal muscle in old rats. *J Gerontol A Biol Sci Med Sci*. 2002;57(10):B366-74.

- Caroni P. Overexpression of growth-associated proteins in the neurons of adult transgenic mice. *J Neurosci Methods*. 1997;71(1):3-9.
- Chen YZ, Bennett CL, Huynh HM, et al. DNA/RNA helicase gene mutations in a form of juvenile amyotrophic lateral sclerosis (ALS4). *Am J Hum Genet*. 2004;74(6):1128-35.
- Clement AM, Nguyen MD, Roberts EA, et al. Wild-type nonneuronal cells extend survival of SOD1 mutant motor neurons in ALS mice. *Science*. 2003;302(5642):113-7.
- Cleveland JL. A new piece of the ALS puzzle. *Nat Genet*. 2003;34(4):357-8.
- Cleveland DW, Rothstein JD. From Charcot to Lou Gehrig: deciphering selective motor neuron death in ALS. *Nat Rev Neurosci*. 2001;2(11):806-19.
- Colombrita C, Onesto E, Megiorni F, et al. TDP-43 and FUS RNA-binding proteins bind distinct sets of cytoplasmic messenger RNAs and differently regulate their post-transcriptional fate in motoneuron-like cells. *J Biol Chem*. 2012;287(19):15635-47.
- D'Ambrogio A, Buratti E, Stuani C, et al. Functional mapping of the interaction between TDP-43 and hnRNP A2 in vivo. *Nucleic Acids Res*. 2009;37(12):4116-26.

Dal Canto MC, Gurney ME. Development of central nervous system pathology in a murine transgenic model of human amyotrophic lateral sclerosis. *Am J Pathol.* 1994;145(6):1271-9.

DeJesus-Hernandez M, Mackenzie IR, Boeve BF, et al. Expanded GGGGCC hexanucleotide repeat in noncoding region of C9ORF72 causes chromosome 9p-linked FTD and ALS. *Neuron.* 2011;72(2):245-56.

Deng HX, Chen W, Hong ST, et al. Mutations in UBQLN2 cause dominant X-linked juvenile and adult-onset ALS and ALS/dementia. *Nature.* 2011;477(7363):211-5.

Elden AC, Kim HJ, Hart MP, et al. Ataxin-2 intermediate-length polyglutamine expansions are associated with increased risk for ALS. *Nature.* 2010;466(7310):1069-75.

Esmaili MA, Panahi M, Yadav S, Hennings L, Kiaei M. Premature death of TDP-43 (A315T) transgenic mice due to gastrointestinal complications prior to development of full neurological symptoms of amyotrophic lateral sclerosis. *Int J Exp Pathol.* 2013;94(1):56-64.

Feng G, Mellor RH, Bernstein M, et al. Imaging neuronal subsets in transgenic mice expressing multiple spectral variants of GFP. *Neuron.* 2000;28(1):41-51.

- Freibaum BD, Chitta RK, High AA, Taylor JP. Global analysis of TDP-43 interacting proteins reveals strong association with RNA splicing and translation machinery. *J Proteome Res.* 2010;9(2):1104-20.
- Galic M, Tsai FC, Collins SR, Matis M, Bandara S, Meyer T. Dynamic recruitment of the curvature-sensitive protein ArhGAP44 to nanoscale membrane deformations limits exploratory filopodia initiation in neurons. *Elife.* 2014;3:e03116.
- Gendron TF, Rademakers R, Petrucelli L. TARDBP mutation analysis in TDP-43 proteinopathies and deciphering the toxicity of mutant TDP-43. *J Alzheimers Dis.* 2013;33 Suppl 1:S35-45.
- Gitcho MA, Baloh RH, Chakraverty S, et al. TDP-43 A315T mutation in familial motor neuron disease. *Ann Neurol.* 2008;63(4):535-8.
- Gitcho MA, Bigio EH, Mishra M, et al. TARDBP 3'-UTR variant in autopsy-confirmed frontotemporal lobar degeneration with TDP-43 proteinopathy. *Acta Neuropathol.* 2009;118(5):633-45.
- Guo Y, Wang Q, Zhang K, et al. HO-1 induction in motor cortex and intestinal dysfunction in TDP-43 A315T transgenic mice. *Brain Res.* 2012;1460:88-95.

Hatzipetros T, Bogdanik LP, Tassinari VR, et al. C57BL/6J congenic Prp-TDP43A315T mice develop progressive neurodegeneration in the myenteric plexus of the colon without exhibiting key features of ALS. *Brain Res.* 2014;1584:59-72.

Ho SN, Hunt HD, Horton RM, Pullen JK, Pease LR. Site-directed mutagenesis by overlap extension using the polymerase chain reaction. *Gene.* 1989;77(1):51-9.

Igaz LM, Kwong LK, Chen-plotkin A, et al. Expression of TDP-43 C-terminal Fragments in Vitro Recapitulates Pathological Features of TDP-43 Proteinopathies. *J Biol Chem.* 2009;284(13):8516-24.

Janssens J, Wils H, Kleinberger G, et al. Overexpression of ALS-associated p.M337V human TDP-43 in mice worsens disease features compared to wild-type human TDP-43 mice. *Mol Neurobiol.* 2013;48(1):22-35.

Johnson BS, Snead D, Lee JJ, Mccaffery JM, Shorter J, Gitler AD. TDP-43 is intrinsically aggregation-prone, and amyotrophic lateral sclerosis-linked mutations accelerate aggregation and increase toxicity. *J Biol Chem.* 2009;284(30):20329-39.

Johnson JO, Pioro EP, Boehringer A, et al. Mutations in the Matrin 3 gene cause familial amyotrophic lateral sclerosis. *Nat Neurosci.* 2014;17(5):664-6.

- Jones CT, Brock DJ, Chancellor AM, Warlow CP, Swingler RJ. Cu/Zn superoxide dismutase (SOD1) mutations and sporadic amyotrophic lateral sclerosis. *Lancet*. 1993;342(8878):1050-1.
- Julien JP. Amyotrophic lateral sclerosis. unfolding the toxicity of the misfolded. *Cell*. 2001;104(4):581-91.
- Kabashi E, Valdmanis PN, Dion P, et al. TARDBP mutations in individuals with sporadic and familial amyotrophic lateral sclerosis. *Nat Genet*. 2008;40(5):572-4.
- Koliatsos VE, Clatterbuck RE, Winslow JW, Cayouette MH, Price DL. Evidence that brain-derived neurotrophic factor is a trophic factor for motor neurons in vivo. *Neuron*. 1993;10(3):359-67.
- Kwiatkowski TJ, Bosco DA, Leclerc AL, et al. Mutations in the FUS/TLS gene on chromosome 16 cause familial amyotrophic lateral sclerosis. *Science*. 2009;323(5918):1205-8.
- Kühnlein P, Sperfeld AD, Vanmassenhove B, et al. Two German kindreds with familial amyotrophic lateral sclerosis due to TARDBP mutations. *Arch Neurol*. 2008;65(9):1185-9.

- Hadano S, Hand CK, Osuga H, et al. A gene encoding a putative GTPase regulator is mutated in familial amyotrophic lateral sclerosis 2. *Nat Genet.* 2001;29(2):166-73.
- Henderson CE, Phillips HS, Pollock RA, et al. GDNF: a potent survival factor for motoneurons present in peripheral nerve and muscle. *Science.* 1994;266(5187):1062-4.
- Johnson JO, Mandrioli J, Benatar M, et al. Exome sequencing reveals VCP mutations as a cause of familial ALS. *Neuron.* 2010;68(5):857-64.
- Kriz J, Gowing G, Julien JP. Efficient three-drug cocktail for disease induced by mutant superoxide dismutase. *Ann Neurol.* 2003;53(4):429-36.
- Lagier-Tourenne C, Cleveland DW. Rethinking ALS: the FUS about TDP-43. *Cell.* 2009;136(6):1001-4.
- Laird FM, Farah MH, Ackerley S, et al. Motor neuron disease occurring in a mutant dynactin mouse model is characterized by defects in vesicular trafficking. *J Neurosci.* 2008;28(9):1997-2005.
- Lambrechts D, Storkebaum E, Morimoto M, et al. VEGF is a modifier of amyotrophic lateral sclerosis in mice and humans and protects motoneurons against ischemic death. *Nat Genet.* 2003;34(4):383-94.

- Lee EB, Lee VM, Trojanowski JQ. Gains or losses: molecular mechanisms of TDP43-mediated neurodegeneration. *Nat Rev Neurosci.* 2012;13(1):38-50.
- Lefebvre S, Bürglen L, Reboullet S, et al. Identification and characterization of a spinal muscular atrophy-determining gene. *Cell.* 1995;80(1):155-65.
- Liu-Yesucevitz L, Bilgutay A, Zhang YJ, et al. Tar DNA binding protein-43 (TDP-43) associates with stress granules: analysis of cultured cells and pathological brain tissue. *PLoS ONE.* 2010;5(10):e13250.
- Lomen-Hoerth C, Anderson T, Miller B. The overlap of amyotrophic lateral sclerosis and frontotemporal dementia. *Neurology.* 2002;59(7):1077-9.
- Ludolph AC, Jesse S. Evidence-based drug treatment in amyotrophic lateral sclerosis and upcoming clinical trials. *Ther Adv Neurol Disord.* 2009;2(5):319-26.
- Mackenzie IR, Bigio EH, Ince PG, et al. Pathological TDP-43 distinguishes sporadic amyotrophic lateral sclerosis from amyotrophic lateral sclerosis with SOD1 mutations. *Ann Neurol.* 2007;61(5):427-34.
- Mackenzie IR, Neumann M, Bigio EH, et al. Nomenclature and nosology for neuropathologic subtypes of frontotemporal lobar degeneration: an update. *Acta Neuropathol.* 2010;119(1):1-4.

- Maruyama H, Morino H, Ito H, et al. Mutations of optineurin in amyotrophic lateral sclerosis. *Nature*. 2010;465(7295):223-6.
- McHanwell S, Biscoe TJ. The sizes of motoneurons supplying hindlimb muscles in the mouse. *Proc R Soc Lond, B, Biol Sci*. 1981;213(1191):201-16.
- Moreira MC, Klur S, Watanabe M, et al. Senataxin, the ortholog of a yeast RNA helicase, is mutant in ataxia-ocular apraxia 2. *Nat Genet*. 2004;36(3):225-7.
- Mortazavi A, Williams BA, Mccue K, Schaeffer L, Wold B. Mapping and quantifying mammalian transcriptomes by RNA-Seq. *Nat Methods*. 2008;5(7):621-8.
- Münch C, Sedlmeier R, Meyer T, et al. Point mutations of the p150 subunit of dynactin (DCTN1) gene in ALS. *Neurology*. 2004;63(4):724-6.
- Narayanan RK, Mangelsdorf M, Panwar A, Butler TJ, Noakes PG, Wallace RH. Identification of RNA bound to the TDP-43 ribonucleoprotein complex in the adult mouse brain. *Amyotroph Lateral Scler Frontotemporal Degener*. 2013;14(4):252-60.
- Neumann M, Sampathu DM, Kwong LK, et al. Ubiquitinated TDP-43 in frontotemporal lobar degeneration and amyotrophic lateral sclerosis. *Science*. 2006;314(5796):130-3.

- Oosthuysen B, Moons L, Storkebaum E, et al. Deletion of the hypoxia-response element in the vascular endothelial growth factor promoter causes motor neuron degeneration. *Nat Genet.* 2001;28(2):131-8.
- Ou SH, Wu F, Harrich D, García-martínez LF, Gaynor RB. Cloning and characterization of a novel cellular protein, TDP-43, that binds to human immunodeficiency virus type 1 TAR DNA sequence motifs. *J Virol.* 1995;69(6):3584-96.
- Parker SJ, Meyerowitz J, James JL, et al. Endogenous TDP-43 localized to stress granules can subsequently form protein aggregates. *Neurochem Int.* 2012;60(4):415-24.
- Pollier J, Rombauts S, Goossens A. Analysis of RNA-Seq data with TopHat and Cufflinks for genome-wide expression analysis of jasmonate-treated plants and plant cultures. *Methods Mol Biol.* 2013;1011:305-15.
- Polymenidou M, Lagier-tourenne C, Hutt KR, et al. Long pre-mRNA depletion and RNA missplicing contribute to neuronal vulnerability from loss of TDP-43. *Nat Neurosci.* 2011;14(4):459-68.
- Pugdahl K, Fuglsang-frederiksen A, De carvalho M, et al. Generalised sensory system abnormalities in amyotrophic lateral sclerosis: a European multicentre study. *J Neurol Neurosurg Psychiatr.* 2007;78(7):746-9.

- Puls I, Jonnakuty C, Lamonte BH, et al. Mutant dynactin in motor neuron disease. *Nat Genet.* 2003;33(4):455-6.
- Rabinovici GD, Miller BL. Frontotemporal lobar degeneration: epidemiology, pathophysiology, diagnosis and management. *CNS Drugs.* 2010;24(5):375-98.
- Raynaud F, Janossy A, Dahl J, et al. Shank3-Rich2 interaction regulates AMPA receptor recycling and synaptic long-term potentiation. *J Neurosci.* 2013;33(23):9699-715.
- Raynaud F, Moutin E, Schmidt S, et al. Rho-GTPase-activating protein interacting with Cdc-42-interacting protein 4 homolog 2 (Rich2): a new Ras-related C3 botulinum toxin substrate 1 (Rac1) GTPase-activating protein that controls dendritic spine morphogenesis. *J Biol Chem.* 2014;289(5):2600-9.
- Renton AE, Majounie E, Waite A, et al. A hexanucleotide repeat expansion in C9ORF72 is the cause of chromosome 9p21-linked ALS-FTD. *Neuron.* 2011;72(2):257-68.
- Richnau N, Aspenström P. Rich, a rho GTPase-activating protein domain-containing protein involved in signaling by Cdc42 and Rac1. *J Biol Chem.* 2001;276(37):35060-70.

- Rollason R, Korolchuk V, Hamilton C, Jepson M, Banting G. A CD317/tetherin-RICH2 complex plays a critical role in the organization of the subapical actin cytoskeleton in polarized epithelial cells. *J Cell Biol.* 2009;184(5):721-36.
- Rosen DR, Siddique T, Patterson D, et al. Mutations in Cu/Zn superoxide dismutase gene are associated with familial amyotrophic lateral sclerosis. *Nature.* 1993;362(6415):59-62.
- Rothstein JD. Of mice and men: reconciling preclinical ALS mouse studies and human clinical trials. *Ann Neurol.* 2003;53(4):423-6.
- Rothstein JD, Patel S, Regan MR, et al. Beta-lactam antibiotics offer neuroprotection by increasing glutamate transporter expression. *Nature.* 2005;433(7021):73-7.
- Rowland LP, Shneider NA. Amyotrophic lateral sclerosis. *N Engl J Med.* 2001;344(22):1688-700.
- Rutherford NJ, Zhang YJ, Baker M, et al. Novel mutations in TARDBP (TDP-43) in patients with familial amyotrophic lateral sclerosis. *PLoS Genet.* 2008;4(9):e1000193.
- Sephton CF, Cenik C, Kucukural A, et al. Identification of neuronal RNA targets of TDP-43-containing ribonucleoprotein complexes. *J Biol Chem.* 2011;286(2):1204-15.

Sieben A, Van Langenhove T, Engelborghs S, et al. The genetics and neuropathology of frontotemporal lobar degeneration. *Acta Neuropathol.* 2012;124(3):353-72.

Shan X, Chiang PM, Price DL, Wong PC. Altered distributions of Gemini of coiled bodies and mitochondria in motor neurons of TDP-43 transgenic mice. *Proc Natl Acad Sci USA.* 2010;107(37):16325-30.

Smith BN, Ticozzi N, Fallini C, et al. Exome-wide rare variant analysis identifies TUBA4A mutations associated with familial ALS. *Neuron.* 2014;84(2):324-31.

Sreedharan J, Blair IP, Tripathi VB, et al. TDP-43 mutations in familial and sporadic amyotrophic lateral sclerosis. *Science.* 2008;319(5870):1668-72.

Stallings NR, Puttaparthi K, Luther CM, Burns DK, Elliott JL. Progressive motor weakness in transgenic mice expressing human TDP-43. *Neurobiol Dis.* 2010;40(2):404-14.

Stribl C, Samara A, Trümbach D, et al. Mitochondrial dysfunction and decrease in body weight of a transgenic knock-in mouse model for TDP-43. *J Biol Chem.* 2014;289(15):10769-84.

Su AI, Wiltshire T, Batalov S, et al. A gene atlas of the mouse and human protein-encoding transcriptomes. *Proc Natl Acad Sci USA.* 2004;101(16):6062-7.

Subramaniam JR, Lyons WE, Liu J, et al. Mutant SOD1 causes motor neuron disease independent of copper chaperone-mediated copper loading. *Nat Neurosci.* 2002;5(4):301-7.

Swarup V, Phaneuf D, Bareil C, et al. Pathological hallmarks of amyotrophic lateral sclerosis/frontotemporal lobar degeneration in transgenic mice produced with TDP-43 genomic fragments. *Brain.* 2011;134(Pt 9):2610-26.

Theys PA, Peeters E, Robberecht W. Evolution of motor and sensory deficits in amyotrophic lateral sclerosis estimated by neurophysiological techniques. *J Neurol.* 1999;246(6):438-42.

Tollervey JR, Curk T, Rogelj B, et al. Characterizing the RNA targets and position-dependent splicing regulation by TDP-43. *Nat Neurosci.* 2011;14(4):452-8.

Truett GE, Heeger P, Mynatt RL, Truett AA, Walker JA, Warman ML. Preparation of PCR-quality mouse genomic DNA with hot sodium hydroxide and tris (HotSHOT). *BioTechniques.* 2000;29(1):52, 54.

Tsai KJ, Yang CH, Fang YH, et al. Elevated expression of TDP-43 in the forebrain of mice is sufficient to cause neurological and pathological phenotypes mimicking FTLD-U. *J Exp Med.* 2010;207(8):1661-73.

Tsao W, Jeong YH, Lin S, et al. Rodent models of TDP-43: recent advances. *Brain Res.* 2012;1462:26-39.

UniProt: a hub for protein information. *Nucleic Acids Res.* 2015;43(Database issue):D204-12.

Van Deerlin VM, Leverenz JB, Bekris LM, et al. TARDBP mutations in amyotrophic lateral sclerosis with TDP-43 neuropathology: a genetic and histopathological analysis. *Lancet Neurol.* 2008;7(5):409-16.

Van Zundert B, Izaurieta P, Fritz E, Alvarez FJ. Early pathogenesis in the adult-onset neurodegenerative disease amyotrophic lateral sclerosis. *J Cell Biochem.* 2012;113(11):3301-12.

Vance C, Rogelj B, Hortobágyi T, et al. Mutations in FUS, an RNA processing protein, cause familial amyotrophic lateral sclerosis type 6. *Science.* 2009;323(5918):1208-11.

Vidal M, Morris R, Grosveld F, Spanopoulou E. Tissue-specific control elements of the Thy-1 gene. *EMBO J.* 1990;9(3):833-40.

Wang Z, Gerstein M, Snyder M. RNA-Seq: a revolutionary tool for transcriptomics. *Nat Rev Genet.* 2009;10(1):57-63.

- Wegorzewska I, Bell S, Cairns NJ, Miller TM, Baloh RH. TDP-43 mutant transgenic mice develop features of ALS and frontotemporal lobar degeneration. *Proc Natl Acad Sci USA*. 2009;106(44):18809-14.
- Wegorzewska I, Baloh RH. TDP-43-based animal models of neurodegeneration: new insights into ALS pathology and pathophysiology. *Neurodegener Dis*. 2011;8(4):262-74.
- Wils H, Kleinberger G, Janssens J, et al. TDP-43 transgenic mice develop spastic paralysis and neuronal inclusions characteristic of ALS and frontotemporal lobar degeneration. *Proc Natl Acad Sci USA*. 2010;107(8):3858-63.
- Wong PC, Pardo CA, Borchelt DR, et al. An adverse property of a familial ALS-linked SOD1 mutation causes motor neuron disease characterized by vacuolar degeneration of mitochondria. *Neuron*. 1995;14(6):1105-16.
- Wong PC, Cai H, Borchelt DR, Price DL. Genetically engineered mouse models of neurodegenerative diseases. *Nat Neurosci*. 2002;5(7):633-9.
- Wu CH, Fallini C, Ticozzi N, et al. Mutations in the proflin 1 gene cause familial amyotrophic lateral sclerosis. *Nature*. 2012;488(7412):499-503.

- Xiao S, Sanelli T, Dib S, et al. RNA targets of TDP-43 identified by UV-CLIP are deregulated in ALS. *Mol Cell Neurosci*. 2011;47(3):167-80.
- Xu YF, Gendron TF, Zhang YJ, et al. Wild-type human TDP-43 expression causes TDP-43 phosphorylation, mitochondrial aggregation, motor deficits, and early mortality in transgenic mice. *J Neurosci*. 2010;30(32):10851-9.
- Xu YF, Zhang YJ, Lin WL, et al. Expression of mutant TDP-43 induces neuronal dysfunction in transgenic mice. *Mol Neurodegener*. 2011;6:73.
- Xu YF, Prudencio M, Hubbard JM, et al. The pathological phenotypes of human TDP-43 transgenic mouse models are independent of downregulation of mouse Tdp-43. *PLoS ONE*. 2013;8(7):e69864.
- Yang Y, Hentati A, Deng HX, et al. The gene encoding alsin, a protein with three guanine-nucleotide exchange factor domains, is mutated in a form of recessive amyotrophic lateral sclerosis. *Nat Genet*. 2001;29(2):160-5.
- Yokoseki A, Shiga A, Tan CF, et al. TDP-43 mutation in familial amyotrophic lateral sclerosis. *Ann Neurol*. 2008;63(4):538-42.
- Zhang HX, Tanji K, Mori F, Wakabayashi K. Epitope mapping of 2E2-D3, a monoclonal antibody directed against human TDP-43. *Neurosci Lett*. 2008;434(2):170-4.

Zhu S, Stavrovskaya IG, Drozda M, et al. Minocycline inhibits cytochrome c release and delays progression of amyotrophic lateral sclerosis in mice. *Nature*. 2002;417(6884):74-8.

CURRICULUM VITAE

William Wei-Liang Tsao

Johns Hopkins University School of Medicine,
Department of Pathology,
558 Ross Building, 720 Rutland Ave.
Baltimore, MD 21205
E-mail: wtsao1@jhmi.edu
Tel: 973-722-2210

Born September 12, 1984, in Taipei, Taiwan.

EDUCATION

Johns Hopkins School of Medicine M.D., Ph.D. in Cellular and Molecular Medicine	Baltimore, MD Expected May 2015
Johns Hopkins University B.S. in Biomedical Engineering / Materials Science	Baltimore, MD May 2006

RESEARCH EXPERIENCE

P. Wong Laboratory, JHU Neuropathology Graduate Student	Baltimore, MD 08/2008 – Present
D. Kerr Laboratory, JHU Institute for Cellular Engineering Graduate Rotation Student	Baltimore, MD 06/2007 – 08/2007
K. Hristova Laboratory, Materials Science, JHU Undergraduate Researcher	Baltimore, MD 01/2004 – 08/2006
T. Minko Laboratory, Ernest Mario School, Rutgers Undergraduate Researcher	New Brunswick, NJ 06/2003 – 08/2003

TEACHING EXPERIENCE

Mammalian Histology Course Biochemistry, Cellular and Molecular Biology Department Teaching Assistant	Baltimore, MD 04/2012
The Human Body Course Cellular and Molecular Medicine Department Teaching Assistant	Baltimore, MD 2010-2011

PUBLICATIONS / ABSTRACTS

Tsao W, Jeong YH, Lin S, Ling J, Price DL, Chiang P, Wong PC. Rodent models of TDP-43: Recent advances. *Brain Research*. 2012;1462: 26-39.

Pakunlu RI, Wang Y, **Tsao W**, Pozharov V, Cook TJ, Minko T. Enhancement of the Efficacy of Chemotherapy for Lung Cancer by Simultaneous Suppression of Multidrug Resistance and Antiapoptotic Cellular Defense: Novel Multicomponent Delivery System. *Cancer Research*. 2004; 64: 6214-24.

Wang Y, Pakunlu RI, **Tsao W**, Pozharov V, Minko T. Bimodal Effect of Hypoxia in Cancer: Role of Hypoxia Inducible Factor in Apoptosis. *Molecular Pharmaceutics*. 2004; 1(2):156-165.

MEETING PRESENTATIONS

Tsao W, Hu A, Wong PC. Neuronal expression of ALS-linked TDP-43 in mice is sufficient to cause adult-onset motor neuron disease. Program No. Z36.54.21. Washington, DC: Society for Neuroscience, 2011.

AWARDS AND HONORS

Richard J. Johns Award, JHU Biomedical Engineering	05/2006
Achievement Award, JHU Materials Science and Engineering	05/2006
Ford Scholarship, Golden Key International Honor Society	05/2004
Merit Award, National Society of Collegiate Scholars	09/2003